

A Review of Phototransistors Using Metal Oxide Semiconductors: Research Progress and Future Directions

Hyukjoon Yoo, I. Sak Lee, Sujin Jung, Sung Min Rho, Byung Ha Kang, and Hyun Jae Kim*

Metal oxide thin-film transistors have been continuously researched and mass-produced in the display industry. However, their phototransistors are still in their infancy. In particular, utilizing metal oxide semiconductors as phototransistors is difficult because of the limited light absorption wavelength range and persistent photocurrent (PPC) phenomenon. Numerous studies have attempted to improve the detectable light wavelength range and the PPC phenomenon. Here, recent studies on metal oxide phototransistors are reviewed, which have improved the range of light wavelengths and the PPC phenomenon by introducing an absorption layer of oxide or non-oxide hybrid structure. The materials of the absorption layer applied to absorb long-wavelength light are classified into oxides, chalcogenides, organic materials, perovskites, and nanodots. Finally, next-generation convergence studies combined with other research fields are introduced and future research directions are detailed.

as memory and sensor applications, as shown in Figure 1.^[16–20]

With the recent development of the internet of things (IoT), sensor technology has attracted immense attention. In particular, photo sensor technology is required to connect users and surrounding objects. Since photosensors are used in automobiles, smart homes, and mobile devices, they are drawing attention as a leader in recent IoT technologies. From the viewpoint of the research trend of photosensors, the main issues include the sensitivity and range of wavelengths that can be absorbed. Accordingly, various materials with semiconductor properties capable of absorbing light are being studied as base materials for photosensors.^[21–24] Figure 2a shows the research

1. Introduction

Currently, we are living in the age of electronics. Since the first development of transistors in 1947,^[1] the semiconductor era has evolved, and the field of silicon-based transistors has made remarkable progress. Transistors have developed in various directions, among which thin-film transistors (TFTs) have been applied to display applications such as liquid crystal displays and organic light-emitting diode displays, and have been continuously studied.^[2–7] Initially, TFTs were fabricated based on amorphous silicon (a-Si); however, the limitation of low mobility was noted as a chronic disadvantage.^[8,9] This problem reached a new turning point as indium gallium zinc oxide (IGZO), which has a higher mobility and lower off-current than a-Si, was developed by the Hosono research group in 2004.^[10] Since the development of IGZO, metal oxide semiconductors have been steadily researched and has been mass-produced in the display industry since 2012. However, research on improving the performance of metal oxide TFTs has been continuously conducted for a long period of time and has reached saturation.^[11–15] Therefore, researchers are constantly attempting to apply metal oxide semiconductors to new applications beyond displays such

trends and market size of photosensors studied over the last 10 years based on searches on Google Scholar and Web of Science. Research papers on photosensors have steadily increased every year, and thus, the scale applied to the industry has also increased; therefore, the market size of photosensors was recorded to be 38.5 billion dollars in 2019. In particular, organic, oxide, 2D materials, and perovskite-based photosensors are mainly studied as the base material, and 2D-material-based semiconductors occupy a high proportion. However, issues such as low carrier mobility or difficulty in large-area deposition still exist for previously studied organic materials and 2D materials. Therefore, attempts have been made to utilize metal oxide TFTs, which facilitate the deposition on large area with high mobility and low off-current, as phototransistors.

Figure 2b shows the research trends on oxide TFTs and metal oxide phototransistors from 2004 to 2019 based on Google Scholar and Web of Science searches. Starting with the IGZO study in 2004, oxide TFT research steadily increased until 2014, and a certain level of research has since been maintained. In contrast, in the case of metal oxide phototransistors, a relatively low number of studies were initially attempted; however, the number of studies has sharply increased since 2015. This indicates the interest of researchers in applying oxide TFTs to phototransistors. However, over the entire period, research on metal oxide phototransistors is only 2.48% of the number of studies on oxide TFTs. Interest in the research on metal oxide phototransistors has increased; however, few studies have yet been conducted, and research reviews have not been properly covered. Most existing phototransistor-related reviews focus on organic, 2D, and perovskite materials,^[25–29] and few have been reviewed in detail yet, focusing on the prospects and advantages

H. Yoo, I. S. Lee, S. Jung, S. M. Rho, B. H. Kang, Prof. H. J. Kim
School of Electrical and Electronic Engineering
Yonsei University
50 Yonsei-ro, Seodaemun-gu, Seoul 03722, Republic of Korea
E-mail: hjk3@yonsei.ac.kr

 The ORCID identification number(s) for the author(s) of this article can be found under <https://doi.org/10.1002/adma.202006091>.

DOI: 10.1002/adma.202006091

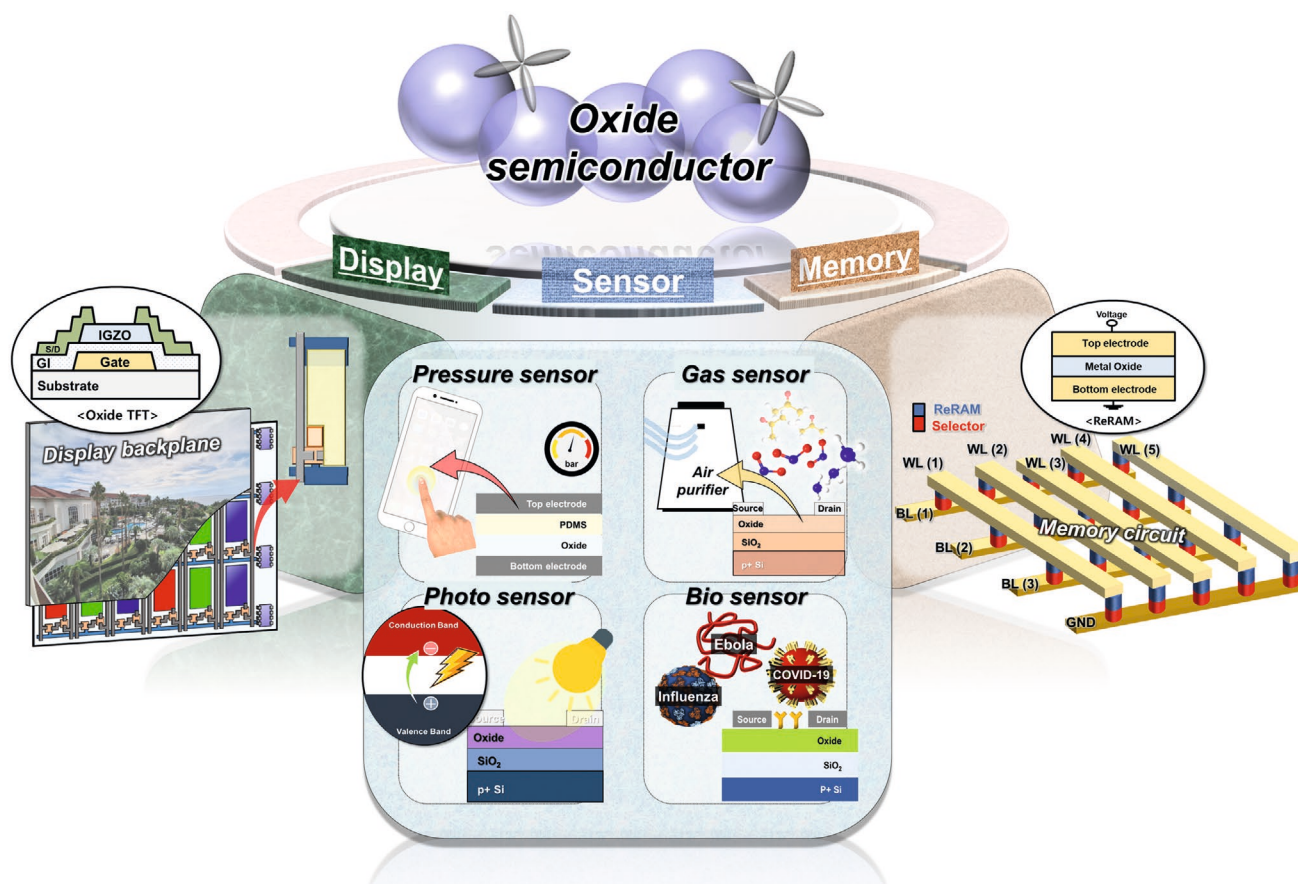


Figure 1. Schematic illustration of the various application using oxide semiconductor; sensor, display backplane, and memory.

of metal oxide phototransistors. Therefore, for the first time, we will review metal oxide phototransistor research in detail.

Herein, recent studies on metal oxide phototransistors are summarized, and leading studies of each technology are introduced. Section 2 describes the material physics of the oxide semiconductors (Section 2.1.) and the basic principles of phototransistors (Section 2.2.). In Section 3, the recent research on metal oxide phototransistors is categorized according to the material of the absorption layer and detailed. This section deals with oxide-absorption-layer-based phototransistors (Section 3.1.) and phototransistors using hybrid structures of non-oxide materials and metal oxide semiconductors (Section 3.2.). In addition, next-generation convergence research combined with other fields by developing phototransistor research will be introduced in Section 4. Finally, we summarize the latest issues in Section 5, anticipate the prospects of this technology, and propose future research directions.

2. Fundamental Principle of Metal Oxide Phototransistors

2.1. Metal Oxide Semiconductors

This section introduces the materials and physical properties of metal oxide semiconductors, which have recently attracted

attention as channel materials for phototransistors. In particular, band formation and electron transport mechanisms of semiconductors are examined in detail. In addition, the representative deposition methods for oxide semiconductors and emerging applications including sensors and memories are introduced.

2.1.1. Material Physics

Oxide TFTs demonstrate a high electrical performance compared with Si-based semiconductors, even in the amorphous phase.^[10,30,31] This characteristics could be explained by the relatively small decrease in electrical performances that was due even in amorphous material, which was due to the orbital structure.^[32] In other words, the key to explaining these phenomena is to clearly understand the physical and chemical concept of “ionic bonding” of metal oxide semiconductors and not the “covalent bonding” of Si materials. In the case of ionic bonding configuration of metal oxide semiconductors, when the charge exchange between metal cations and oxide anion occurs, the external s-orbital of the metal ions is empty, and the external p-orbital of oxygen ions is filled as shown in Figure 3a. Charge exchange occurs at the “Madelung potential,” which divides the metal and oxygen ion orbitals, with the empty s-orbitals of the metal cation predominantly forming the

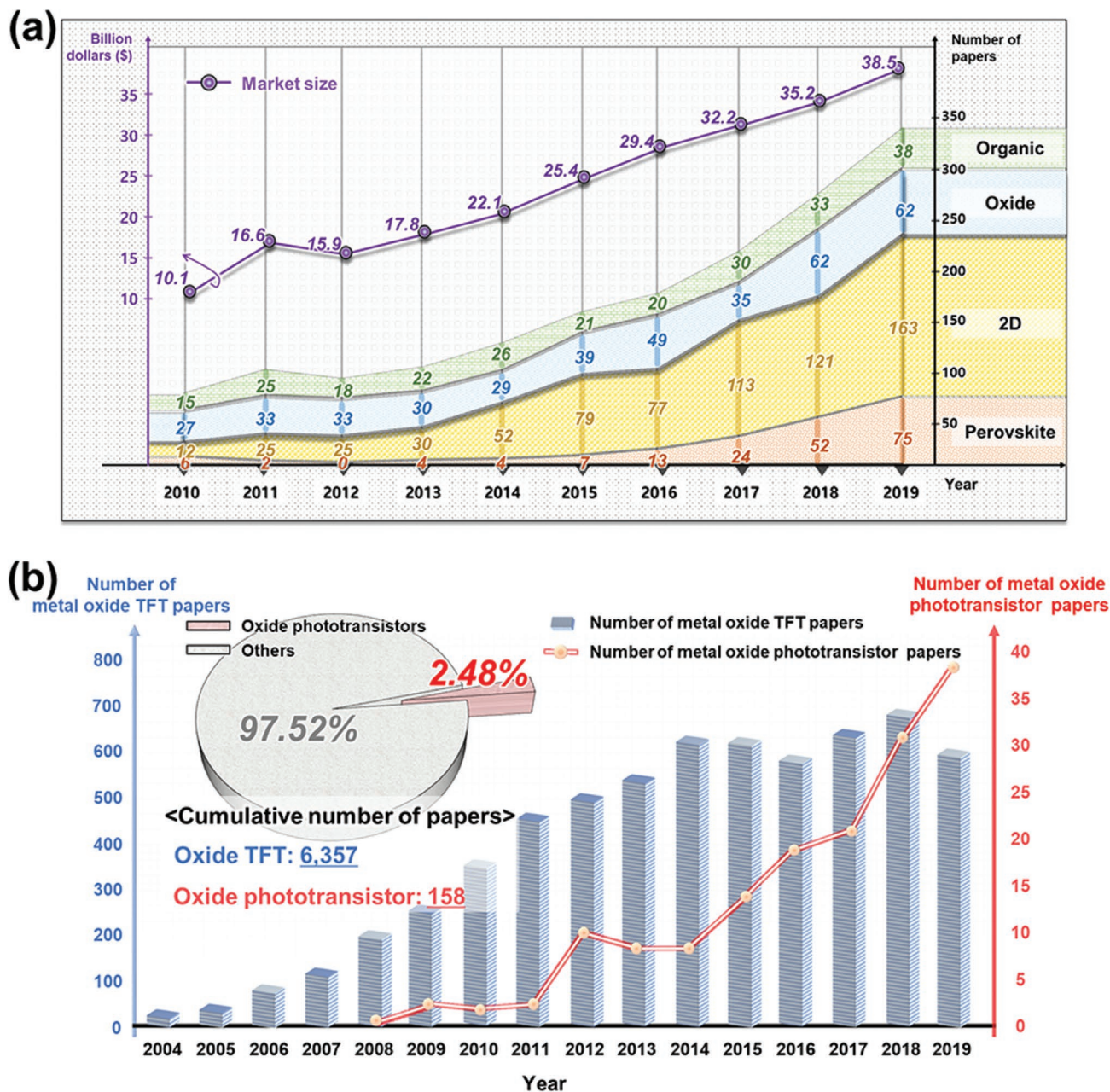


Figure 2. a) The number of the photosensor papers according to materials of the TFT's channel layer published from 2010 to 2019, based on Web of Science searches and global market size of photosensor from 2010 to 2019. (IHS 2019). b) The number of the metal oxide TFT and metal oxide phototransistor papers published from 2004 to 2019, based on Google Scholar and Web of Science searches. Percentage of the number of metal oxide phototransistors to the number of the oxide TFT papers. (The detailed search conditions with categories are shown in Figures S1, S2, and S3 in the Supporting Information.)

bottom of the conduction band, and the filled p-orbitals of the oxygen anion mainly forming the top of the valence band as shown in Figure 3b. According to this mechanism of band formation, metal oxide materials have a wide bandgap (>3.0 eV) in the ultraviolet (UV) range.^[33] Figure 3c is a schematic diagram of the orbital structure in the crystal phase. The conduction band of the metal oxide semiconductor is mainly formed by the overlapping of the metal ns orbitals showing isotropic properties due to spherical symmetry, which is known as a conduction

path for free electrons that can be formed along the overlapped metal ns orbitals. As shown in Figure 3d, the spherical symmetry of the ns orbitals renders the metal oxide material insensitive to structural distortion, and the metal oxide semiconductor has high electron mobility even in the amorphous state. Compared with Si-based TFTs, which undergo a significant decrease in mobility from 1000 (single crystal phase) to 1 (amorphous phase) $\text{cm}^2 \text{V}^{-1} \text{s}^{-1}$, in contrast, there is little difference in mobility between the crystal and amorphous

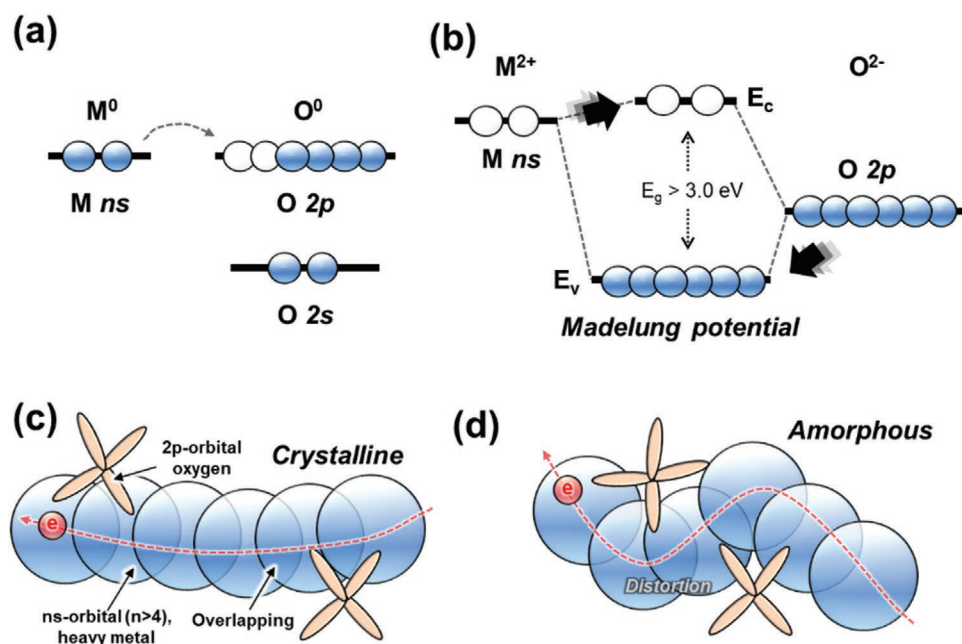


Figure 3. a,b) Schematic diagrams of bandgap formation mechanisms in metal oxide semiconductor before (a) and after (b) ionic bonding. M^0 and O^0 mean metal and oxygen molecules in a neutral state. M^{2+} is a metal cation that has lost electrons, and O^{2-} is an oxygen anion that has obtained electrons. c,d) Carrier transport paths of metal oxide semiconductors according to phase: c) crystalline and d) amorphous.

phases in metal oxide TFTs.^[10] Therefore, since metal oxide semiconductors do not require an additional crystallization process, the fabrication process of oxide TFTs is less complicated than that of Si-based TFTs.^[34]

2.1.2. Representative Deposition Methods

Various fabrication methods have been developed for depositing oxide semiconductor thin films. Sputtering, atomic layer deposition, and evaporation techniques have been developed as representative vacuum deposition methods, and the sol-gel technique is continuously being studied for solution-based processes.^[35–38] In this section, we introduce the representative oxide semiconductor deposition methods, sputtering process, and sol-gel process.

Sputtering Process: The sputtering is one of the most widely employed vacuum processes for material deposition methods in electrodes, insulators, and semiconductors. Sputtering refers to the physical removal of atoms from the surface of the target material by the collision of energetic particles (i.e., an ionized gas known as plasma) on the surface of materials.^[39,40] These atoms removed from the target surface by this energy bombardment are transferred to the adjacent surface (i.e., substrate), thus depositing a film of the desired thickness. The sputtering method has several advantages: 1) it can deposit various metals, insulators, alloys, and composites, 2) the film quality and step coverage are better than those of evaporation, 3) uniformity large-area deposition is achieved, and 4) the thermal damage due to room temperature deposition is minimized. Because of these advantages, the sputtering process for metal-oxide materials is widely utilized.

Sol-Gel Process: The sol-gel method is one of the most widely used solution processes for oxide material deposition. The sol-gel method uses a solution or a gel as an intermediate step (i.e., chemical reaction, hydrolysis, and condensation reaction) to convert a molecular precursor in a liquid state into a solid oxide network to form a thin film.^[41] The sol-gel method is classified as either full-area deposition or selective area deposition. Spin-coating, dip-coating, and chemical bath deposition are mainly used for full area deposition, whereas the printing process is used for selective area deposition.^[30,42] These sol-gel methods have several advantages: 1) the fabrication of various composite materials by applying the stoichiometry of the desired reagents, 2) cost efficiency because there is no need for vacuum equipment, and 3) deposition of only selected areas (i.e., printing method) to simplify the process steps.

2.2. Phototransistor

Photosensors are generally classified as photodiodes, photoconductors, and phototransistors.^[43,44] Photodiodes and photoconductors are two-terminal devices in which a photoactive material is connected to two electrodes (as shown in **Figure 4a,b**). A photodiode and a photoconductor are operated by collecting photogenerated carriers in the electrodes during light irradiation. The photodiode is constructed based on p-n or Schottky junctions and has a vertical structure; in contrast, a photoconductor is constructed based on the Ohmic junction, and has a lateral structure. If the lifetime of the photogenerated carriers is shorter than the time required to reach the electrodes, recombination occurs before the photogenerated carriers are collected on the electrode, because of which the device

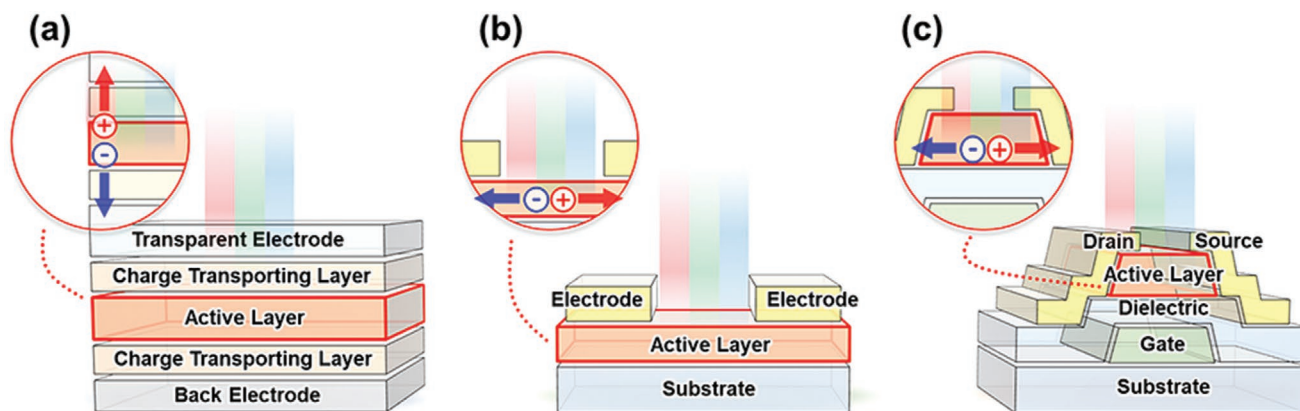


Figure 4. a–c) Schematic illustrations of the structures of different photosensors: a) photodiode, b) photoconductor, and c) phototransistor.

does not work.^[43] Therefore, photodiodes with the vertical structure are used more often than photoconductors with the lateral structure because the distance between electrodes for the vertical structure is shorter.^[27,45] The structure of phototransistors is the same as that of TFTs with three electrodes: source, drain, and gate (Figure 4c). Like a two-terminal device, the device is operated by collecting photogenerated carriers that move along the active channel layer. In particular, the amount of drain current flowing through the accumulated channel can be controlled by the magnitude of the gate bias.^[46] Recently, it has been noted that phototransistors, which can amplify the output signal through voltage control of a gate electrode, exhibit advantages in fabricating high-performance photosensors. Therefore, we will focus on phototransistors in this review.

2.2.1. Operation Mechanism

Phototransistors are operated by generating a photocurrent when the active channel layer located laterally between the source and drain is irradiated with light. Unlike photodiodes which have a vertical structure, the channel length of phototransistors is relatively long; therefore, carrier mobility becomes an important factor.^[27] In general, photocurrent is generated through charge photogeneration and carrier-transport processes.

Charge Photogeneration: When the light energy is larger than the bandgap of a material, the material absorbs the light energy and generates electron–hole pairs.^[47] Since most amorphous oxide semiconductors have a bandgap energy of ≈ 3.0 eV, band-to-band electron–hole pair generation occurs by light absorption when irradiated below UV wavelengths ($\lambda < 400$ nm). In contrast, when light with a long wavelength ($\lambda > 400$ nm) is incident, band-to-band electron–hole pair generation does not occur because the light cannot be absorbed. However, if there are various sub-gap states due to defects in the bandgap, electrons could be excited to the conduction band through the states, or the defect states could be ionized to generate free electrons, resulting in relatively low levels of electron–hole pairs even in long-wavelength light.^[48–51]

Carrier Transport: Since the basic structure of oxide phototransistors is the same as that of the oxide TFTs, oxide phototransistors operate in two driving modes—depletion and

accumulation. When considering an oxide-semiconductor-based n-type channel, the transistor is operated in the depletion mode under a negative bias. Therefore, electrons are pushed out of the channel/gate insulator interface to suppress the channel current. In contrast, transistors are operated in an accumulation mode under a positive gate bias; therefore the channel current increases by electrons accumulated at the channel/gate insulator interface. When charge photogeneration occurs by light irradiation, the photovoltaic effect or photoconductive effect is observed depending on the operating mode of the transistor.^[52,53] In the depletion mode, light induces a photoconductive effect, and the photocurrent of the phototransistor linearly increases with the intensity of the irradiated light.^[54] In contrast, in the accumulation mode, the photovoltaic effect is dominant in the phototransistor; thus, the threshold voltage (V_{th}) of the phototransistor is shifted.^[55–57] Photogenerated holes accumulate near the source electrode by gate and drain bias to lower the electron injection barrier between the source and the semiconductor channel, thereby facilitating electron injection. The reduction in the electron injection barrier by light irradiation induces a negative shift of V_{th} and contributes to an increase in channel current.

2.2.2. Figures of Merit

In addition to the electrical parameters of the TFT, such as field effect mobility, subthreshold swing (S.S), V_{th} , and on/off current ratio, phototransistors have several optoelectronic parameters representing photoreactivity and efficiency.

Photoresponsivity: Photoresponsivity (PR) is defined as the photocurrent flowing through the phototransistor for unit incident light power. The unit of PR is amperes/watts ($A W^{-1}$), and it is calculated as follows^[28]

$$PR = \frac{J_{photo}}{P} \quad (1)$$

where J_{photo} is the photocurrent density, and P is the power of incident light. The photocurrent density is calculated by dividing the difference between I_{photo} and I_{dark} by the unit area, where I_{photo} is the total current in the presence of light, and I_{dark} is the current in the absence of light.

Photosensitivity: Photosensitivity (P) is the measure of the optical switching ratio between the channel current of the phototransistor and the channel current in the dark state when irradiated with light. Since it is a ratio of currents, it does not have a unit; it is calculated as follows^[27]

$$P = \frac{I_{\text{photo}} - I_{\text{dark}}}{I_{\text{dark}}} \quad (2)$$

Specific Detectivity: Specific detectivity (D^*) is an indicator of the degree of weakening of the light being detected. The detectivity is determined by the photoresponsivity of the phototransistor, device active area, and noise level. The unit of D^* is Jones, and it is defined as follows^[26,27]

$$D^* = \frac{PR\sqrt{A}}{S_n} = \frac{PR}{\sqrt{2q}I_{\text{dark}}} \quad (3)$$

where PR is the photoresponsivity, A is the active area of the phototransistor, and S_n is the noise spectral density, which generally includes shot noise, flicker noise, Johnson noise, and $1/f$ noise. The noise spectral density is calculated as follows, assuming that the shot noise is dominant in a high-bandgap device: $S_n = \sqrt{2qI_{\text{dark}}}$.^[27,58,59]

External Quantum Efficiency: The external quantum efficiency (EQE) is the number of photoinduced carriers that are detected per incident photon. It is defined as the ratio of the number of extracted photogenerated charge carriers to the number of incident photons. EQE uses % as a unit and is defined as follows:^[27,28]

$$\text{EQE} = \frac{J_{\text{photo}}/q}{P/h\nu} \quad (4)$$

where q is the electron charge, and $h\nu$ is the photon energy. In the case of photodiodes, an absorbed photogenerated electron generates only one electron/hole pair; thus, the EQE cannot be higher than 100%. In contrast, in phototransistors with ohmic contact, when a hole moves slower than an electron or is trapped in a device, other electrons are injected until the hole reaches the electrode or recombines to maintain charge neutrality. Therefore, more than one electron can flow by a single absorbed photon, resulting in an EQE of more than 100%.^[60–65]

2.2.3. Limitations of Metal Oxide Phototransistors

Oxide-semiconductor-based phototransistors can generate high photocurrents with excellent photocarrier transmission capability because of their higher carrier mobility than that of conventional organic materials or a-Si-based phototransistors. In addition, a low off-current has the advantage of increasing the ratio of I_{photo} and I_{dark} to obtain high photosensitivity. However, oxide semiconductor-based phototransistors also have the following two limitations.

First, owing to the wide bandgap, most oxide semiconductors are transparent in the visible light region; thus, oxide semiconductors can be employed in applications such as transparent displays. However, transparency is also a limitation to

their use in phototransistors. As shown in **Figure 5a**, most oxide semiconductors with a high bandgap energy of ≈ 3.0 eV can absorb UV light. However, since they cannot absorb long-wavelength light, their use in sensors that detect visible light or infrared (IR) is limited. Therefore, in order to solve this problem, researchers are attempting to widen the detection wavelength by introducing an absorption layer having a low bandgap energy or forming sub-gap states in the energy band of the oxide semiconductor.

First, when an absorption layer is applied, a heterojunction structure is formed by laminating a material having a lower bandgap energy than that of an oxide semiconductor as shown in **Figure 5b**. At this time, the energy difference of conduction band between the two materials is not large, whereas the valence band has a large energy difference, so a potential barrier must be formed. The reason is that the photoinduced electrons generated in the absorption layer move to the oxide semiconductor along the conduction band, while the photoinduced hole cannot move to the oxide semiconductor by the potential barrier, thereby suppressing recombination. As another method, when forming sub-gap states in the energy band of oxide semiconductor, electrons in the valence band can be excited as conduction bands by riding the states in the bandgap under light illumination as shown in **Figure 5c**. That is, the bandgap of the oxide semiconductor is substantially reduced, so that the oxide semiconductor can directly absorb light in a long wavelength range.

Second, metal oxide phototransistors show serious limitations that are detrimental to real-time photodetection. As shown in **Figure 5d**, even after the optical input signal disappears, the persistent photocurrent (PPC) phenomenon occurs in metal oxide phototransistors in which a high photocurrent is caused which is steadily maintained. The PPC is affected by the defect distribution, as follows^[64]

$$I_{\text{DS}}(t) = I_{\text{DS}}(0) \left[\exp \left\{ - (t/\tau)^\beta \right\} \right] \quad (5)$$

where $I_{\text{DS}}(0)$ is the current at the onset of decay, β is the distribution of defects that control the decay process, and τ is the relaxation time. In the case of oxide semiconductors, when the oxygen vacancy (V_o) in the thin film is irradiated by light, it is ionized to V_o^+ or V_o^{++} , which acts as a trap site and seriously affects the PPC phenomenon, as shown in **Figure 5e**. Electrons generated by the ionized V_o cause the energy of the localized defect state to move up to near the conduction band, increasing the channel conductivity, giving rise to PPC.^[65,66] Without the supply of sufficient external activation energy, spontaneous recombination and transition to neutral V_o do not occur.^[51,66–68] Therefore, recently, researchers have been conducting a lot of research on suppressing PPC by removing defects related to ionized oxygen vacancies by applying a gate bias pulse while turning off light as shown in **Figure 5f**.

3. Classification of Metal Oxide Phototransistors by Absorption Layer

To overcome the material limitations of oxides, various studies have recently been conducted. Attempts have been made to

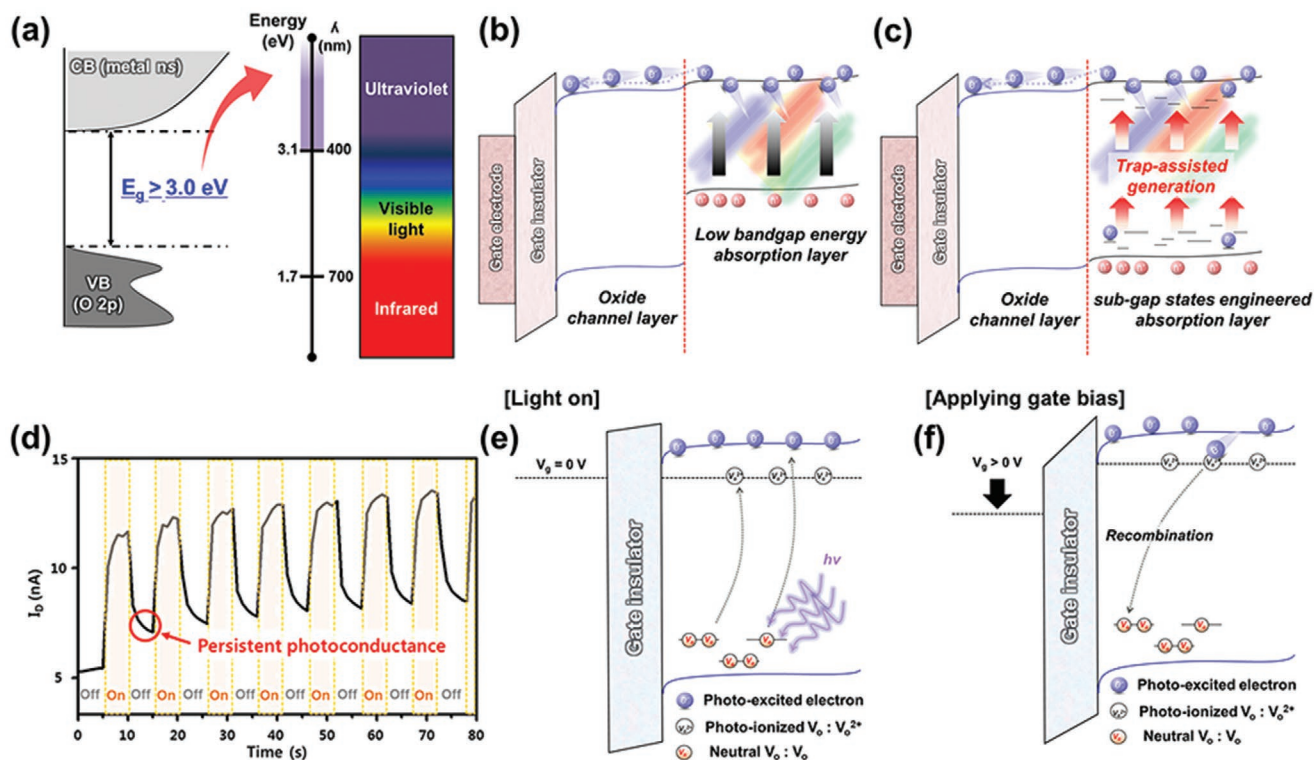


Figure 5. a) Limitation of light absorption range due to wide bandgap energy. b) Photosensing mechanism of oxide phototransistor by application of low bandgap energy absorption layer. c) Photosensing mechanism of oxide phototransistor by sub-gap states engineering in oxide semiconductor. d) The PPC phenomenon occurring in oxide-semiconductor-based phototransistors. e, f) Schematic band diagrams: e) occurrence of PPC issue due to ionized oxygen vacancy, f) alleviation of PPC issue by applying gate bias. d) Reproduced with permission.^[69] Copyright 2018, American Chemical Society.

improve the light detection capability through subsequent processes for oxides or to introduce new materials as an absorption layer. As materials for the absorption layer, oxides, chalcogenides, organic substances, perovskite, and nanodots are mainly studied. **Figure 6** shows the number of papers and authors from 2010 to 2019 based on Google Scholar and Web of Science searches according to the material of “the absorption layer” additionally applied to the metal oxide phototransistor. The graph is divided into two regions—oxide and others—because of the large difference in their scales. Thus, the bubble size of oxides was reduced to 1/10 of the respective original size. The highest number of papers and authors were found for oxides. In contrast, research on applying other absorption layer materials, including chalcogenide, organic, perovskite, and nanodots, in a hybrid structure is still lesser than that on single oxides. In other words, research on applying new materials as an absorption layer is still insufficient, and it is a field that requires further research. In this section, we will introduce the latest research trends of metal oxide phototransistors based on classifying them by absorption layer material.

3.1. Absorption Layers Based on Oxide Materials

As previously mentioned, oxide TFTs have the advantages of high carrier mobility and low off-current, but it is difficult to absorb light in the wavelength range of 400 nm or more, and

the PPC phenomenon occurs. This section introduces studies in which light absorption wavelength range and PPC issues have been improved through structural and process engineering by applying oxide semiconductors as single-layer or a multilayer structures for light absorption layers.

3.1.1. Oxide Single-Layer

Recently, in order to enhance the PPC phenomenon and the detection of wavelengths, some techniques have been developed to modify the oxide single layer.^[51,68,69] Among them, surface treatment techniques have decreased the PPC phenomenon. Kang et al. demonstrated a method to reduce the PPC issue by sequential surface treatment, which includes pre-annealing, UV–ozone treatment, and post-annealing treatment as shown in **Figure 7a**.^[72] In each step, the ZnO film was affected in three effects by the treatment: 1) pre-annealing treatment improved the surface uniformity of the ZnO film and reduced the residual solvent, 2) UV–ozone treatment decreased the oxygen vacancy, and 3) post-annealing treatment refined the ZnO film density and induced zinc–oxygen bonding. Owing to the improved film quality, the photoelectric recovery time after the irradiation of the UV light was shortened, indicating that the PPC effect on the ZnO phototransistor is decreased as shown in **Figure 7b**.

Another approach proposed by Ding et al. involved an IGZO TFT-based phototransistor with Al₂O₃ gate dielectric deposited

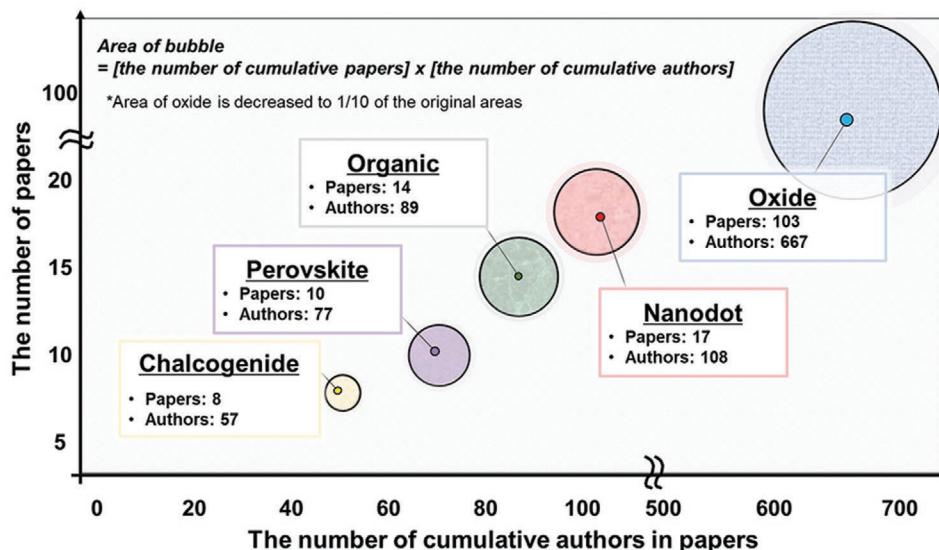


Figure 6. The number of papers and authors on the materials of “absorption layer” additionally applied to the metal oxide phototransistor from 2010 to 2019. Area of bubble means that product of the number of cumulative papers and the number of cumulative authors. The detailed search conditions with categories about metal oxide phototransistors are shown in Figure S3 in the Supporting Information).

by plasma-enhanced atomic layer deposition to expand the detection range.^[73] Figure 7c shows a schematic illustration of the IGZO TFT with a hydrogen-rich Al_2O_3 dielectric and hydrogen ions diffused channel layer. According to this report, the hydrogen ion in Al_2O_3 are released into the IGZO film during the sputtering process, causing hydrogen doping in the film; therefore, the IGZO film could induce sub-gap states in the IGZO bandgap. To verify this, they demonstrated the transfer characteristics of the phototransistor at a fixed light intensity of $50 \mu\text{W cm}^{-2}$ with various wavelengths ranging from 300 to 700 nm as shown in Figure 7d. As the light wavelength decreased, the drain current of the phototransistor gradually increased; even in the visible light region, it is possible to react to light. Moreover, the IGZO phototransistor exhibited a high photoresponsivity of over $6 \times 10^5 \text{ A W}^{-1}$ and a large light-to-dark current ratio of up to 10^7 .

In addition, several research groups have overcome the limitations of phototransistors by engineering structures of phototransistors, in contrast to the previous approaches which involved surface treatment or diffusion techniques.^[75–78] Sze et al. chose a single layer of indium zinc oxide (IZO) thin film as the active layer for both detection of visible light and improvement of the PPC phenomenon and showed that the structure of phototransistors and biasing gate voltage were optimized.^[79] To improve the sensing characteristics such as detection region and optical responsivity, they optimized the channel structure, and the transfer characteristics of the phototransistor are shown in Figure 7e. In the transfer characteristics, it was confirmed that the optimized phototransistor could detect the wavelength of green light that was not previously detected. This reveals that the off-state drain current exhibits an obvious change according to the channel structure (i.e., the ratio of channel width and length), especially under the light illumination. More clearly, the off-state drain current is dominated by light-induced current, which consists of

excess carrier concentration (ionized oxygen vacancies) by the light-excited generation in the IZO channel layer as shown in Figure 7f. Second, they demonstrated that a positive gate pulse was applied to phototransistors to accelerate the recoverability of electrical characteristics from the adverse effects of PPC, as shown in Figure 7g. Through this, as shown in Figure 7h, the electrons are gathered toward the gate insulator, which pushes the trapped electrons and acts as additional energy for recombination. Accordingly, the phototransistor returns to the state before receiving the light. Furthermore, it also proves that the PPC phenomenon can be overcome through deployment of a positive gate pulsing scheme within a few microseconds. In addition, there are various technologies for engineering the gate insulator of phototransistors. Most studies have involved changing the state of the interface between the channel and the gate insulator or controlling the gate insulator material itself.

A different approach to overcoming the issues of metal oxide phototransistors is doping technique in the channel layer. For example, Chang et al. showed that Mg-doped ZnO phototransistor could achieve a responsivity as high as 3.12 A W^{-1} under -5 V and 290 nm UV, which proves that Mg doping could passivate the oxygen related defects in the channel layer and improve the responsivity.^[80]

3.1.2. Oxide Multilayer

Phototransistors based on oxide semiconductor single-layers exhibit improved PPC phenomenon and sensitivity in the visible light region; however, they still have a narrow limit in the sensible wavelength range. Accordingly, to further improve the sensitivity of visible light, studies have been conducted to design the structure of the oxide channel layer from a conventional single layer to a multilayer.^[81–88] In these studies, an oxide material capable of absorbing visible light was introduced

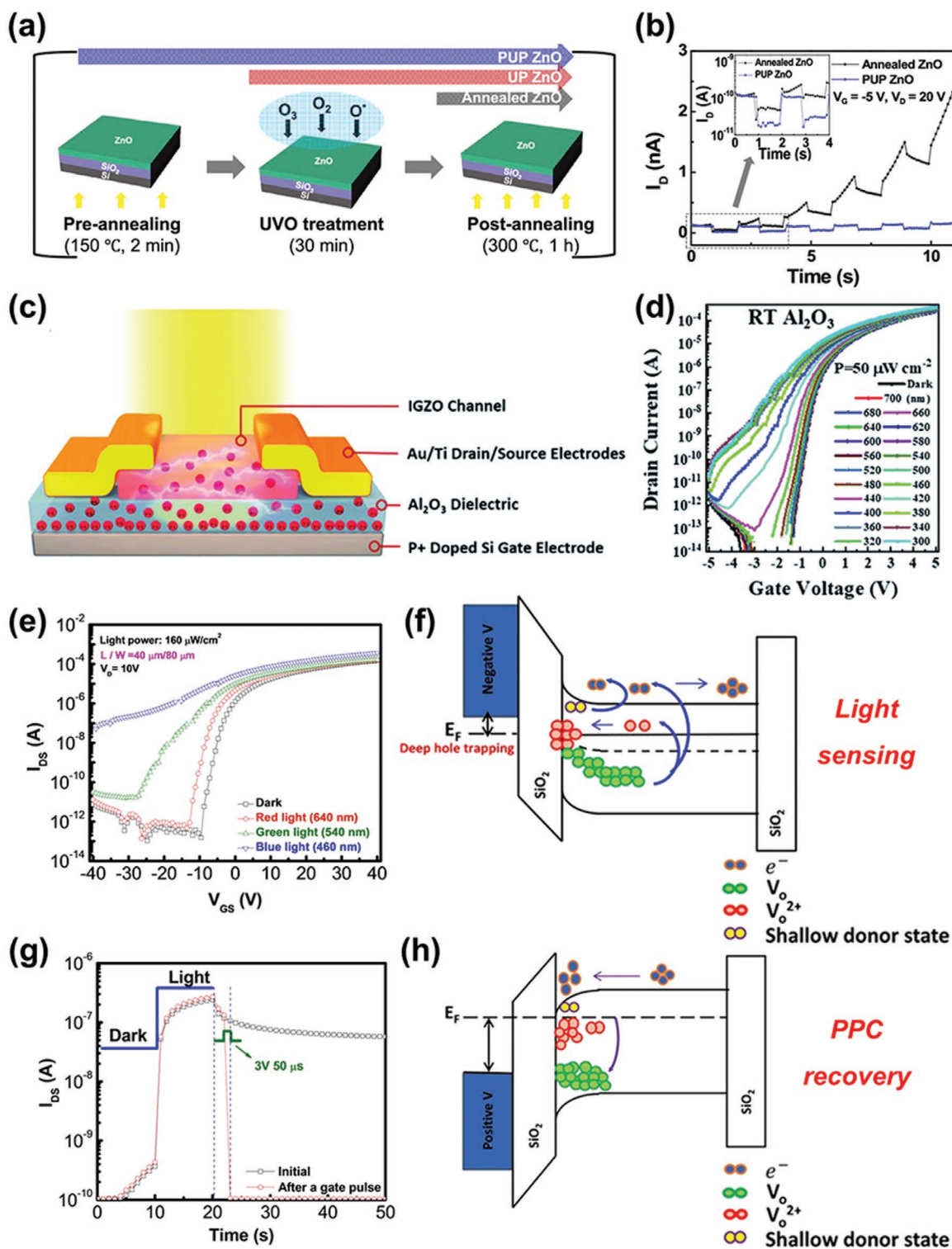


Figure 7. a) Schematic illustration of the sequential surface treatment of ZnO films. b) Periodic photoresponses of ZnO phototransistors under irradiation of light (405 nm and 0.5 Hz). The inset shows the graph on a log scale for the initial 4 s. a,b) Reproduced with permission.^[72] Copyright 2019, American Chemical Society. c) Schematic diagram of IGZO film with hydrogen rich Al₂O₃ dielectric structure. d) Transfer characteristics of the IGZO TFT with hydrogen rich Al₂O₃ dielectric. c,d) Reproduced with permission.^[73] Copyright 2019, Royal Society of Chemistry. e) Transfer characteristics of IZO sensor TFT with a fixed ratio of channel length (i.e., 40 μm/80 μm). f) Schematic band diagram of the a-IZO sensor TFT, which conceptually depicts the mechanism of blue-light sensing. g) drain current versus measured time curves of IZO sensor TFT, while a 50 μs positive gate pulse was applied for recovering from PPC to the original dark state. h) Schematic band diagram of the a-IZO sensor TFT, which conceptually depicts the mechanism of positive-bias-assisted PPC recovery. e–h) Reproduced under the terms of the CC-BY Creative Commons Attribution 4.0 International license (<https://creativecommons.org/licenses/by/4.0/>).^[79] Copyright 2018, The Authors, published by Springer Nature.

for the absorption layer or defects in the oxide thin film were controlled to improve the range of the absorption wavelength. In particular, by introducing such a multilayer structure, it was possible to implement both a layer with improved light absorption efficiency and a layer with excellent photoinduced charge transfer characteristics.

Among oxide semiconductors, IGZO, which is commonly used as an active channel layer, has a bandgap energy above 3.0 eV, and thus, it cannot absorb visible light. However, if an oxide semiconductor with a relatively low carrier mobility and low bandgap energy is applied as an absorption layer, light in the visible region can be absorbed. Liu et al. proposed an oxide-semiconductor-based phototransistor with a SnO/IGZO dual structure.^[89] As shown in **Figure 8a**, IGZO was applied as an active channel layer for a carrier transport, and SnO was stacked on top of the IGZO as an absorption layer to absorb visible light. The SnO-capped IGZO phototransistor could absorb 540 nm of green light, as shown in **Figure 8b**, enabling photosensing, and it was confirmed that it recovered stably when the light was blocked. According to **Figure 8c**, when the device is irradiated with light, electron–hole pairs are generated because of absorption of light in SnO, which has a relatively lower bandgap energy than IGZO, and the photogenerated electrons move to the IGZO layer to form a photocurrent. In addition, the ionization of V_o in IGZO and electrons generated in the shallow donor state contribute to the formation of photocurrent.

Studies have also been conducted to improve the range of light absorption wavelengths by controlling the concentration of V_o in thin films. Nathan et al. designed an oxide-semiconductor-based phototransistor in which IZO was doped with hafnium to control the V_o concentration in thin films.^[90] According to **Figure 8d**, the channel layer of the device was composed of an IZO and HIZO heterojunction. The lower HIZO layer was advantageous for photogenerated charge transfer through the low V_o concentration and high mobility, whereas the upper IZO layer maximized the light absorption efficiency due to the high V_o concentration. Therefore, remarkably high visible light detection performance was observed (**Figure 8e**). A high concentration of V_o in the IZO layer was ionized to generate electrons, thereby increasing the visible light absorption rate. In addition, the PPC phenomenon was improved by forcibly recover the current to the initial state by applying a pulse voltage to the gate electrode as shown in **Figure 8f**. Even after the external optical signal was removed, the ionized V_o and photogenerated electrons that could not be spontaneously recombined were forcibly recovered by the positive gate bias, thereby improving the PPC phenomenon. A similar concept was studied by the same research group who studied gallium-doped IZO and IZO heterojunction structure phototransistors.^[91] The fabricated device could absorb of 500 nm green light, and PPC was also reduced by the gate pulse bias. However, the lack of the detection capability for red light was still revealed as a limitation in these studies.

To further improve the visible light detection range of oxide semiconductor, researches controlling the defect states in the metal oxide thin film have been conducted. In general, oxide semiconductors can generate a small photocurrent through the ionization of V_o even when irradiated with photoenergy lower

than the bandgap; however, the effect is insufficient compared to band to band generation. Therefore, it was attempted to increase the photogeneration efficiency by forming sub gap states in the bandgap or defects in the thin film. Kim et al. demonstrated a phototransistor with a double-layered channel structure in which an oxide semiconductor of the same composition was synthesized through different deposition methods.^[92] As shown in **Figure 8g**, a solution-processed IGZO absorption layer (SAL) was deposited on the sputter-processed IGZO phototransistor. The solution process was conducted by spin coating or electrohydrodynamic (EHD) jet printing. SAL formed a thin film that contained several defects by forming residual organic matter in the film through a low-temperature annealing process (200 °C). Thus, as shown in **Figure 8h**, excellent light absorption was confirmed even under red light of 635 nm. This was a result of the efficient transport of photoelectrons through the sputter-processed IGZO layer with high mobility as well as the generation of a large number of photogenerated electrons excited from a plurality of states in the bandgap of SAL (**Figure 8i**). Kim et al. also attempted to improve the absorption efficiency of visible light by controlling the sub-gap states as a process of another concept. In this study, as shown in **Figure 8j**, a hydrogen-doped IGZO absorption layer (HAL) was fabricated through hydrogen plasma doping on the IGZO backchannel.^[67] The HAL applied IGZO phototransistor could obtain a high photoresponsivity of 1008.8 A W⁻¹ in the red light of 635 nm, as shown in **Figure 8k**, similar to the SAL-based IGZO phototransistor introduced earlier. This was interpreted to be a result of the increase in the sub-gap states due to hydrogen doping, which acts as a shallow donor state within the IGZO bandgap, resulting in band to band photogeneration even with visible light energy lower than the bandgap (**Figure 8l**). Moreover, the PPC phenomenon caused by photogenerated electrons trapped at the HAL and IGZO channel interface was solved by forcible recombination by applying a gate pulse bias as shown in **Figure 8m**. Furthermore, Kim et al. studied a phototransistor implementing multilayers of the IGZO channel layer and nanowire-based mesh structure of TiO₂ to engineer the sub-gap state in an oxide semiconductor.^[93] TiO₂ absorbed oxygen from the surrounding IGZO during the annealing process through a higher oxygen bonding strength than IGZO, thus increasing the concentration of V_o in the IGZO film. In particular, because TiO₂ was deposited as a mesh structure, the surface area was maximized and a large number of V_o could be generated. Therefore, by forming a number of defects due to V_o in the IGZO film, during light irradiation, electrons in the valence band rise through the states in the bandgap and generate photoinduced electrons; thus, red and green light can be detected.

In addition to these studies, Cho et al. attempted to sense IR beyond the visible light region by inducing sub-gap states in the channel by stacking Al₂O₃ on the IGZO layer.^[94] Although the photosensitivity was as low as 10², this is a remarkable study in that it attempted to detect an IR of 850 nm based on an oxide semiconductor with a high bandgap energy.

The properties of the metal oxide phototransistors based on the oxide-based absorption layer are listed in **Table 1**. The sensing wavelength and optoelectronic parameters were compared by dividing the categories according to the oxide single-layer or multilayer structure.

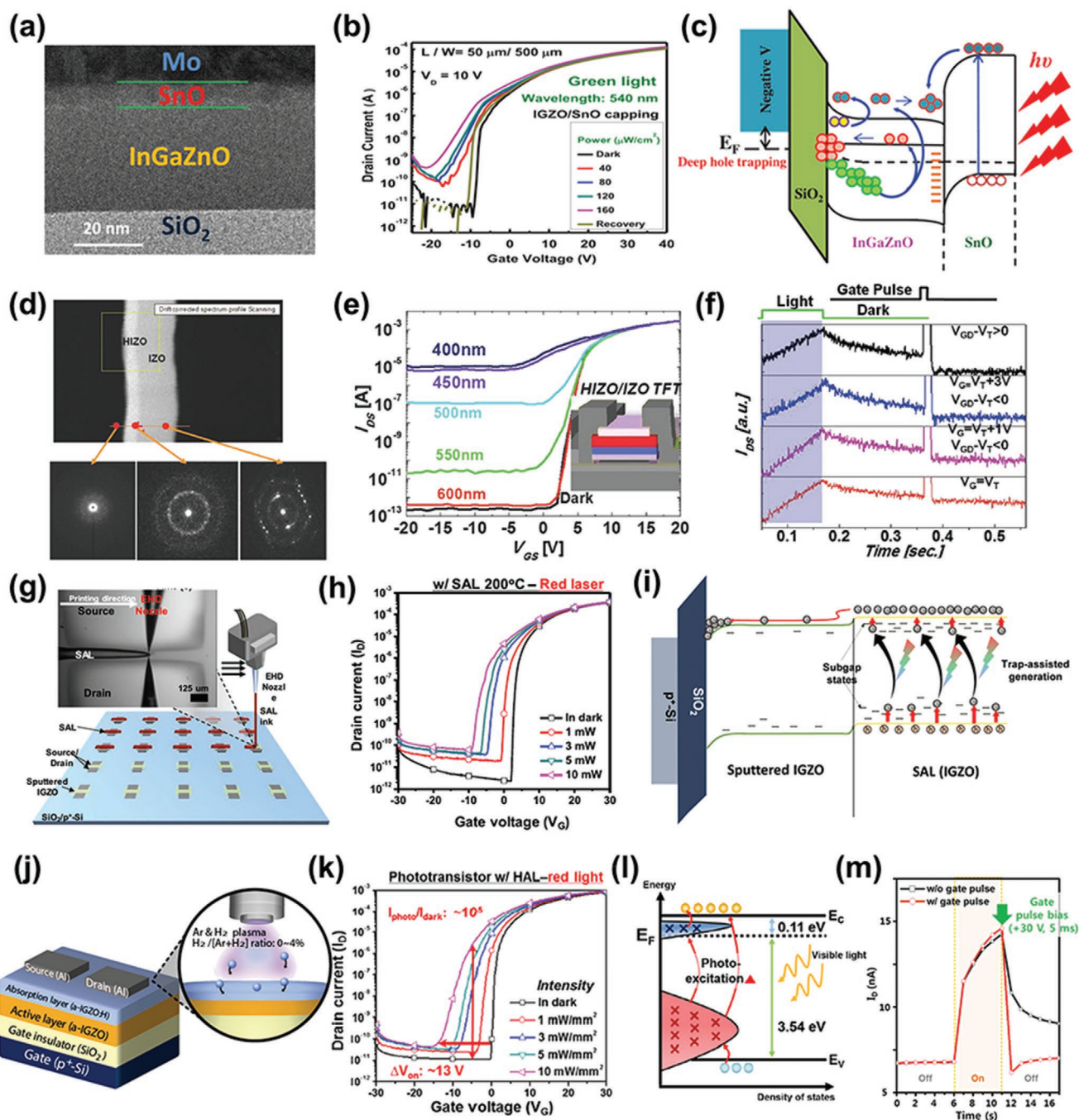


Figure 8. a) Cross-sectional image of IGZO phototransistor capping with SnO absorption layer by transmission electron microscopy. b) Transfer characteristics of IGZO phototransistor capping with SnO absorption layer under 540 nm green light. c) Schematic band diagram of IGZO phototransistor capping with SnO absorption layer under negative gate bias. a–c) Reproduced with permission.^[89] Copyright 2019, Wiley-VCH. d) Cross-sectional image of HIZO-IZO bilayer phototransistor by high-angle annular dark-field scanning transmission electron microscopy. e) Transfer characteristics of HIZO-IZO bilayer phototransistor under illumination with light-wavelength. f) Drain current as a function time when phototransistor receives light pulse and positive bias pulse. d–f) Reproduced with permission.^[90] Copyright 2014, Wiley-VCH. g) Schematic illustration of SAL deposition with EHD printing and nozzle image. The inset shows a detailed printing image. h) Transfer characteristics of the IGZO phototransistor with SAL under red laser (635 nm). i) Schematic illustration of trap-assisted generation and electron transport of IGZO phototransistor with SAL. g–i) Reproduced with permission.^[92] Copyright 2019, American Chemical Society. j) Schematic image of IGZO phototransistor with HAL. k) Transfer characteristics of IGZO phototransistor with HAL under red light illumination (635 nm). l) Schematic illustration of the energy level alignment of IGZO: H for the absorption layer. m) Comparison of one cycle photoresponse characteristics according to gate pulse bias. j–m) Reproduced with permission.^[69] Copyright 2018, American Chemical Society.

Table 1. Reports on the photosensing characteristics according to the structure of the metal oxide absorption layer of the phototransistor.

Category	Figure	Absorption layer	Channel layer	Detection wavelength [nm]	PR [$A W^{-1}$]	P	D^* [Jones]	EQE [%]	Ref.	Published year
Single-layer	7a,b	Same as channel	ZnO	405 – 780	>30	–	–	–	[72]	2019
	7c,d	Same as channel	IGZO	300 – 700	6×10^5	–	–	–	[73]	2020
	7e–h	Same as channel	IZO	460 – 640	1280	10^5	–	–	[79]	2018
	–	Same as channel	IGZO	250 – 400	4.75	–	–	–	[70]	2012
	–	Same as channel	IGZO	250 – 400	3.2	–	–	–	[75]	2013
	–	Same as channel	IGZO	370 – 430	–150	–	–	–	[51]	2016
	–	Same as channel	IGZO	406 – 623	–	–	–	–	[77]	2016
	–	Same as channel	MgZnO	250 – 450	3.12	–	–	–	[80]	2017
	–	Same as channel	IGZO	380 – 385	–	–	–	–	[71]	2018
	–	Same as channel	In ₂ O ₃	300 – 400	$>7 \times 10^3$	2.33×10^5	1.6×10^{16}	3×10^4	[74]	2018
	–	Same as channel	ZnO	300 – 450	2520	–	1.57×10^{11}	>100	[76]	2019
	–	Same as channel	MgGaO	254 – 365	8.9	10^5	–	4.34×10^3	[78]	2019
Multilayer	8a–c	SnO	IGZO	460 – 640	398.02	6.8×10^5	–	–	[89]	2019
	8d–f	Hf:IGZO	IZO	400 – 600	–	–	–	$\sim 10^8$	[90]	2014
	8g–i	IGZO (sol)	IGZO	532 – 635	206	8.34×10^6	4.23×10^{11}	–	[92]	2019
	8j–m	IGZO:H	IGZO	400 – 700	1932.6	3.85×10^6	6.93×10^{11}	–	[69]	2018
	–	IZO	GIZO	400 – 700	$\approx 10^5$	–	–	$\sim 10^4$	[91]	2012
	–	IZO	GIZO	500	–	–	–	–	[81]	2015
	–	Al ₂ O ₃	IGZO	400 – 850	–	$\approx 10^2$	–	–	[94]	2020
	–	TiO ₂	IGZO	405 – 635	178.66	1.04×10^5	1.25×10^{10}	–	[93]	2020

3.2. Absorption Layer Based on Non-Oxide Materials

Many researchers have struggled to widen the detection range of phototransistors with a single oxide material, and in the previous section, we introduced some studies that have attempted to overcome this issue. However, oxide semiconductor materials inherently have a wide bandgap, so there is a limitation to the development of phototransistor improving sensitivity and detection wavelength light using only oxide materials.

To solve these issues, several methods for improving the detection wavelength of metal oxide phototransistors have been reported, which are operated by introducing a wide range detectable absorption layer into the devices. These hybrid-structured phototransistors are composed of a non-oxide absorption layer (i.e., chalcogenide, organic, perovskite, and nanodot materials) on the oxide channel layer. When external light is incident on the hybrid structure, efficient photogeneration occurs by a band-to-band light absorption in the area of the absorption layer, and photocharges are efficiently transferred through an oxide material (i.e., channel layer). Therefore, it is possible to detect a wide wavelength through the phototransistor based on a hybrid structure. From now on, we introduce representative studies on hybrid-structure-based phototransistors using various absorbing layer materials for improving phototransistors.

3.2.1. Chalcogenide Materials

Phototransistors based on chalcogenide/oxide semiconductor hybrid structures in which chalcogenide is applied as an

absorption layer material for improving the light absorption wavelength range have been studied.^[95–97] Chalcogenide is an inorganic compound semiconductor in which anions of Group 16 chalcogen-based elements (selenium, sulfur, tellurium, etc.) and metal cations are combined. Chalcogenide has a bandgap energy which is suitable for absorbing light in the visible light region, and it has been used in various forms such as thin films, 2D flakes, nano-crystals, and nanowires.

Kim et al. reported a phototransistor with a molybdenum sulfide (MoS₂)/IGZO hybrid structure using MoS₂, which is a representative 2D chalcogenide material, as an absorption layer.^[98] The MoS₂ thin film was grown by spin coating and furnace annealing, and then transferred to the top of the IGZO layer to fabricate a device, as shown in Figure 9a. The fabricated phototransistor could absorb and detect light from 405 to 655 nm as shown in Figure 9b. Although it was impossible to detect an IR of 700 nm or more, it was possible to absorb light in the entire visible light region. This is because MoS₂ with a low bandgap of 1.5 eV absorbs light and generates electron–hole pairs, as shown in Figure 9c. The photoinduced electrons move to IGZO and generate a photocurrent. Similar studies using the same material have been conducted by other research groups. Kim et al. studied MoS₂/IGZO hybrid phototransistors using MoS₂ flakes as an absorption layer.^[99] Unlike previously introduced MoS₂ thin film based phototransistors, in this study, MoS₂ flakes were deposited on top of the IGZO layer using a standard adhesive-tape-based method, and the device could detect light in the IR region up to 1100 nm with a photoresponsivity of 14.9 mA W⁻¹.

Studies using another chalcogenide material, cadmium sulfide (CdS) as an absorption layer, have also been reported.

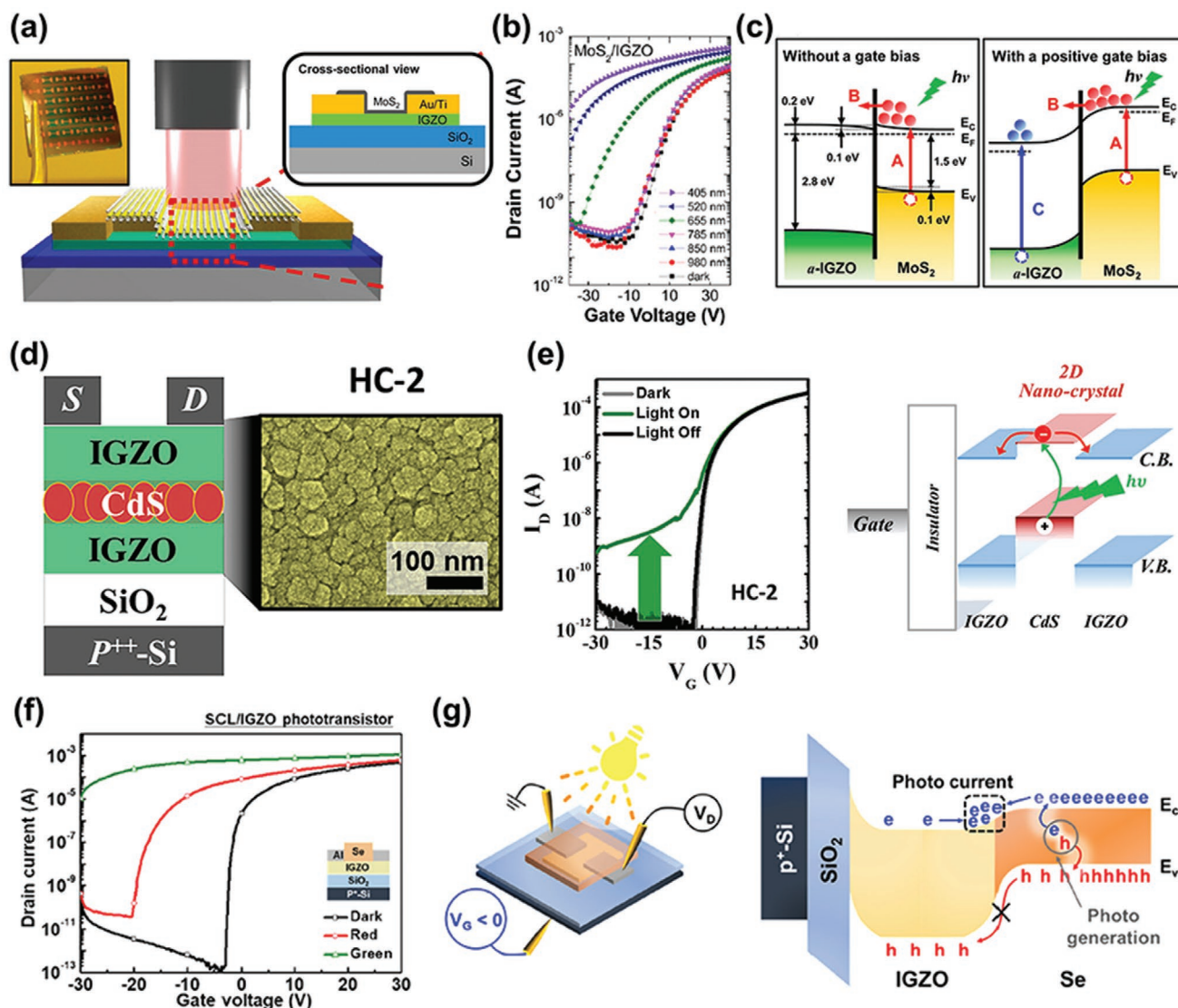


Figure 9. a) Schematic illustration of the MoS₂/IGZO phototransistor. The inset shows an optical microscopy image of an array of MoS₂/IGZO phototransistors. b) Transfer characteristics of MoS₂/IGZO phototransistor as a function of the illuminating light wavelength. c) Schematic illustrations of energy band alignment and photo induced charge transfer mechanism of MoS₂/IGZO stack without and with gate bias. a–c) Reproduced with permission.^[98] Copyright 2016, American Chemical Society. d) Schematic illustration and plan-view images of the CdS/IGZO hybrid channel phototransistors. e) Variation of transfer characteristics of CdS/IGZO hybrid channel phototransistor under green light (550 nm, 2.25 eV) and schematic band diagrams of photosensitivity behavior. d,e) Reproduced with permission.^[99] Copyright 2017, Elsevier Inc. f) Transfer characteristics of SCL/IGZO phototransistor under red (635 nm) and green (532 nm) light illumination. g) Operation mechanism of SCL/IGZO phototransistor based on energy band diagram with positive gate bias under light illumination. f,g) Reproduced with permission.^[103] Copyright 2020, American Chemical Society.

Cho et al. applied CdS to an IGZO phototransistor as a nano-crystal-type absorption layer.^[100] In particular, in this study, the characteristics of the phototransistor according to the location of the CdS absorption layer were compared. Thus, the device structure with the CdS absorption layer located in the middle of the IGZO channel layer, as shown in Figure 9d, exhibited higher light absorption efficiency than those below or above the IGZO layer. The optimized structure of the CdS/IGZO phototransistor showed a photoconductive effect by increasing the off-current when irradiated with light of 550 nm wavelength, as shown in Figure 9e. This was reported to be caused by the maximization of the photocurrent generation by CdS with a

bandgap energy of 2.23 eV, which absorbed light effectively to generate photoinduced electrons and supplied electrons to both the back and front of the IGZO channel. Another study of a similar concept was attempted by the same research group. Cho et al. fabricated a phototransistor with a similar structure in which the absorption layer is located in the channel bulk layer using a coarse nano-crystal CdS and solution-process-based zinc tin oxide channel material.^[101] In this study, a phototransistor capable of detecting all the visible light wavelengths of 650, 550, and 450 nm was developed by maximizing the light wavelength detection area by numerous defect sites. Moreover, in another case, CdS was applied to the absorption layer in

different ways. Liao et al. presented a hybrid phototransistor incorporating an IZO channel and a CdS absorption layer by synthesizing CdS into a nanowire structure and coating it with the IZO solution.^[102] This resulted in improved carrier mobility and photoresponsivity, and the possibility of sensing large-scale visible light images was demonstrated by implementing a sensor array.

Attempts have also been made to apply a single chalcogen material as an absorption layer. Kim et al. reported a selenium capping layer (SCL)/IGZO hybrid phototransistor in which selenium (Se), a representative single-element chalcogen semiconductor, was applied as a visible light absorption layer.^[103] The Se absorption layer deposited by thermal evaporation could absorb light in all visible light regions, as shown in Figure 9f, owing to the low bandgap energy of 1.95 eV. In particular, high photoresponsivity of 328 and 1390 A W⁻¹ were obtained under red and green light irradiation, respectively. As shown in Figure 9g, the electrons formed by photogeneration in Se migrate to IGZO and generate photocurrents, whereas photogenerated holes cannot move to IGZO owing to the difference in the potential barrier, so that recombination is blocked.

3.2.2. Organic Materials

Recently, to overcome the problem of the PPC phenomenon and detection range, dual-channel structures of oxide and organic-hybrid-based phototransistors have been proposed, enabling a wide-detectivity-based photosensor.^[104–107] Historically, charge photogeneration in organic materials is less efficient than their inorganic counterparts because of the strong electron–hole interaction and disordered nature.^[28,108] However, the recent development in organic thin films has significantly improved the charge photogeneration efficiency, with a promising layer achieving wide range photodetection and high sensitivity. Furthermore, the absorption wavelength of thin-film organic photodetectors can be easily tuned by modifying the chemical structure, thereby allowing a wide and tunable spectral range that covers UV–vis, near-infrared (NIR), and even X-ray.

As a simple method for converting a broad bandgap metal oxide phototransistor into a visible light transistor with high sensitivity and fast response, a study on an organic capping layer was proposed by Meng et al.^[109] After capping a polymer with a high visible light absorption coefficient (i.e., poly3-hexylthiophene; P3HT) on to a conventional upper contact lower gate a-IGZO TFT, a significant photocurrent was observed under visible light illumination. The schematic cross-sectional diagram of the device without P3HT capping [that is a standard (STD)] and a capping device are shown in Figure 10a. Figure 10b shows that the conventional metal oxide phototransistor (i.e., IGZO TFT) is apparently blind to visible light, whereas the metal oxide phototransistor capped P3HT absorbs visible light well. They explained this response to visible light because of light-induced electron accumulation in the oxide layer according to the absorption of light in P3HT, as shown in Figure 10c. As a result, electrons accumulated in the oxide layer caused the device V_{th} shift negative direction. This shows the

possibility that if the sensing target can react to light and cause charge transfer to the oxide layer, it can detect wavelengths in a wide range of regions.

Although the photosensitive organic material could be introduced as an absorbing layer for phototransistors, this method still faces issues. The energy bands of some organic materials are too narrow and are located differently, which leads to misalignment between the oxide and the organic material, and consequently, the excited electrons cannot move to the oxide layer. To improve transport to excited electrons, Cao et al. developed an IGZO phototransistors coupled with organic (i.e., PDOT:PSS)-oxide heterojunction by inserting a p-type oxide layer (i.e., SnO_x) between the organic and IGZO layer as shown in Figure 10d.^[110] Figure 10e shows the transfer curves of IGZO and PEDOT:PSS/SnO_x/IGZO TFTs in the dark and under illumination at different wavelengths. In the case of both devices, the transfer curves changed marginally under illumination at $\lambda \geq 550$ nm. More importantly, the light illumination sensitivity of the PEDOT:PSS/SnO_x/IGZO phototransistor was more prominent than that of IGZO TFTs. To explain the enhancement mechanism, the energy band diagram of the PEDOT:PSS/SnO_x/IGZO stack is illustrated in Figure 10f. This figure shows that a built-in electric field (E_b) is indeed generated near the back channel with the electric field direction from IGZO to PEDOT:PSS. Therefore, the photoinduced electron–hole pairs would be separated more efficiently with the help of the built-in electric field, and a larger photocurrent could be generated. This study verified the effect of introducing an organic layer for light absorption, tentatively demonstrating the functionality of the insertion layer for hybrid phototransistors.

In another work, bulk-heterojunction (BHJ)-based research has also been conducted.^[111,112] For example, Yang et al. reported metal oxide phototransistors with high photosensitivity and broad bandwidth response based on the bilayer of organic BHJ materials and an IGZO layer in Figure 10g.^[113] As opposed to the conventional single organic absorption layer, the BHJ consist of low-bandgap conjugated polymer poly [2,6'-4,8-di(5-ethylhexylthienyl)benzo[1,2-b;3,4-b]dithiophene-alt-5-dibutyloctyl-3,6-bis(5-bromothiophen-2-yl)pyrrolo[3,4-c]pyrrole-1,4-dione] (PBDTT-DPP; bandgap ≈ 1.44 eV) and [6,6]-phenyl C61 butyric acid methyl ester (PC₆₁BM). Interestingly, the transfer curves drastically changed even at 780 nm (in the NIR region) and showed a high photosensitivity in the NIR to NUV region as shown in Figure 10h. As a result, this combination of these two organic materials can allow excited electrons in the light absorption layer to better move to the oxide layer in Figure 10i. Moreover, the fabrication temperature of both organic and IGZO layers of the phototransistors is below 250 °C. Hence, they were able to demonstrate flexible phototransistors on polyimide substrates, as shown in Figure 10j. The electrical properties of the devices did not change significantly over 800 cycles with a bending radius of 2.5 mm, confirming the high performance for flexible operations.

3.2.3. Perovskite Materials

Perovskite, which has excellent light absorption efficiency and is particularly used for high-efficiency solar cells, has received

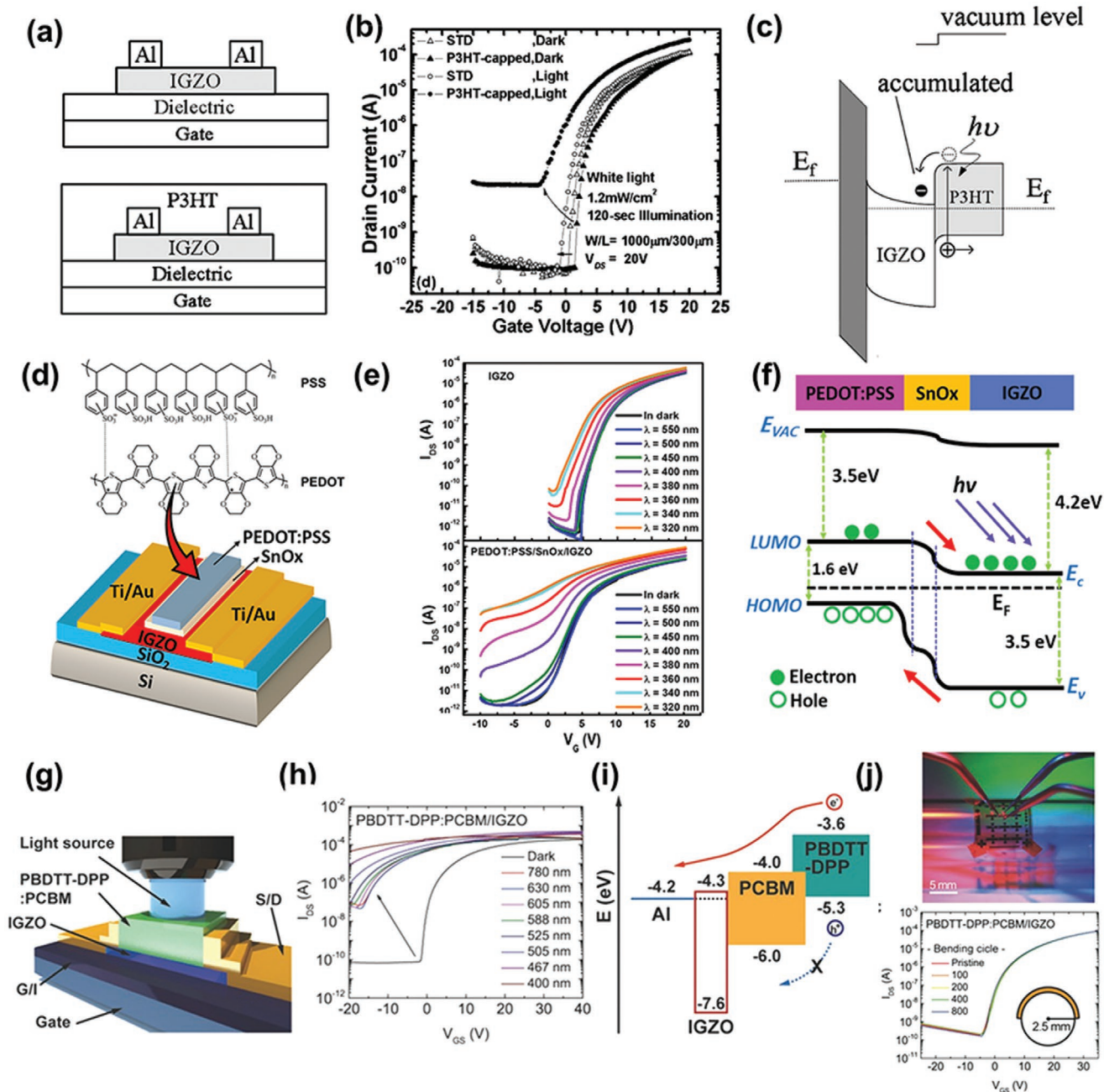


Figure 10. a) Schematic illustration of IGZO TFT and P3HT-capped IGZO TFT. b) Transfer characteristics before and after 120 s white light illumination of IGZO and P3HT-capped a-IGZO TFT. c) Schematic energy-band diagram of the P3HT-capped IGZO TFT near the drain side when light illumination. a–c) Reproduced with permission.^[109] Copyright 2010, American Institute of Physics. d) Schematic diagram of the PEDOT:PSS/SnO_x/IGZ phototransistor and chemical structure of PEDOT:PSS. e) Transfer characteristics of the IGZO and PEDOT:PSS/SnO_x/IGZO phototransistors in the dark or under light illumination. f) Schematic illustration showing the energy band alignment and the photoinduced charge transfer mechanism of the PEDOT:PSS/SnO_x/IGZO stacked structure. d–f) Reproduced with permission.^[110] Copyright 2018, American Chemical Society. g) The device structure of IGZO with PBDTT-DPP:PC₆₁BM layer under the light illumination. h) The transfer characteristics of the PBDTT-DPP:PC₆₁BM/IGZO devices under light illumination. i) Schematic band diagram of the electron and hole transport mechanism between the PBDTT-DPP:PC₆₁BM and IGZO interface. j) Flexible PBDTT-DPP:PC₆₁BM/IGZO phototransistors and bending test of phototransistor with a maximum bending radius of 5 mm. g–j) Reproduced with permission.^[113] Copyright 2019, Wiley-VCH.

increasing amount of interest as an absorbing layer material for phototransistors. Methylammonium lead iodide (MAPbI₃) is a typical organic–inorganic hybrid perovskite, and cesium lead halide (CsPbI₃) or cesium lead bromide (CsPbBr₃) have been

mainly studied as typical inorganic perovskites. Recently, phototransistors with a hybrid structure in which such perovskite is stacked together with an oxide semiconductor have been reported.^[114–119]

In the case of hybrid phototransistors using organic/inorganic perovskite materials, Kim et al. proposed a visible light phototransistor of a MAPbI₃/IGZO hybrid structure.^[120] A MAPbI₃ absorption layer with a bandgap energy of 1.8 eV was deposited on the top of the IGZO thin film by a spin coating process. As shown in Figure 11a, the device absorbed 532 nm green light and showed a photosensitivity of 10⁶. In addition, organic–inorganic perovskite has a disadvantage in that it is impossible to secure long-term stability of the device owing to the issue of high instability in the environment, especially in terms of moisture. In this study, the surface of the MAPbI₃ absorption layer exposed to the atmosphere was protected using an oxide passivation layer. As a result, the phototransistor was stably operated even after water was dropped on the device as shown in Figure 11b. In addition, the PPC phenomenon was significantly improved compared with the phototransistor of the IGZO single layer as shown in Figure 11c. A similar study using MAPbI₃ as an absorption layer was published by Zhou et al., who implemented a phototransistor that could sense from UV (385 nm) to NIR (750 nm) by applying the MAPbI₃ absorption layer to the IGZO phototransistor in a hybrid structure.^[121] In addition, Wu et al. reported that MAPbI₃ could be applied as an absorption layer to both n-type and p-type oxide semiconductors through a phototransistor study in which the MAPbI₃ absorption layer was applied in a hybrid structure with SnO, a p-type oxide semiconductor.^[122]

Attempts have been made to further improve the light absorption efficiency in the conventional MAPbI₃/IGZO hybrid phototransistor. Zhou et al. proposed a structure in which PC₆₁BM is inserted between the MAPbI₃ absorption layer and the IGZO channel layer in the existing hybrid structure, as shown in Figure 11d.^[123] As shown in Figure 11e, the MAPbI₃-IGZO phototransistor with PC₆₁BM inserted could detect visible light and IR at 800 nm. As shown in the section on organic/oxide hybrid structure, PC₆₁BM acts as an electron transport layer, allowing electrons generated by light absorption from MAPbI₃ to be better transferred to IGZO, thus maximizing the light absorption efficiency, as shown in Figure 11f.

As such, MAPbI₃-based organic/inorganic-perovskite-based phototransistors have been studied in various ways; however, because they are vulnerable to moisture, researchers have tried to improve the device stability problem by applying inorganic perovskites. Kim et al. applied CsPbI₃, an inorganic perovskite, as an absorption layer of an IGZO phototransistor and attempted to improve the absorption effect of visible light by doping Br in the CsPbI₃ absorption layer.^[124] As shown in Figure 11g,h, when CsPbI₂Br is used as an absorption layer, the entire visible light region can be detected, in contrast to the conventional device which can detect blue light only. As shown in Figure 11i, the light absorbed by CsPbI₂Br causes electron/hole pair generation, and the electrons move to IGZO to generate a photocurrent.

Liao et al. introduced a CsPbBr₃/IGZO hybrid phototransistor by applying CsPbBr₃ as an absorption layer.^[125] In particular, as shown in Figure 11j, the ITO nanowire was integrated into IGZO to secure a fast response. Thus, it was driven as a phototransistor when exposed to light with a wavelength of 457 nm, as shown in Figure 11k, and a flexible phototransistor

was also implemented by applying the device on a flexible substrate, as shown in Figure 11l.

3.2.4. Nanodot Materials

Nowadays, nanodot materials have stimulated research interests because they combine novel physical properties induced by metallic plasmonic and quantum confinement effects with relatively mature processing techniques. In this section, we introduce two categories of nanodot materials (i.e., metallic plasmonic and quantum dot) for using oxide phototransistors.

Metallic Plasmonic: Integrating noble metal (gold, silver, and platinum) nano-particles (NPs) has been considered another approach to develop phototransistors using a wide bandgap oxide semiconductor for detecting visible and IR regions.^[126–127] For example, Wang et al. fabricated a visible light phototransistor of gold (Au) NPs/IGZO structure as shown in Figure 12a.^[128] When Au NPs were illuminated by incident light, several photoelectrons were excited and then injected into the IGZO layer, such that the drain current of the phototransistor increased under light illumination (658 nm) as shown in Figure 12b. To visualize this phenomenon, Figure 12c shows the local electric field distribution in the longitudinal cross-section of the Au NPs/IGZO film at different wavelengths (405, 532, and 658 nm). Thus, the electric field increased when the device was illuminated by visible light owing to the Ag NPs. Therefore, Au NPs improved the detection wavelength of IGZO phototransistors through surface plasmon resonance.

Quantum Dot: Similarly, the quantum dots (QDs)/metal oxide phototransistors could be easily modified photonic properties by controlling the size of QD particles.^[129–134] For instance, Nathan et al. reported a QD/IGZO phototransistor for detecting visible light region as shown in Figure 12d.^[135] The n-type CdSe QDs modified by the ligand (tri-n-octyl phosphine oxide, TOPO) were utilized as the absorption layer to inject photogenerated electrons into the IGZO layer. As a result, the off-current and V_{th} were fluctuated in the visible and UV wavelength as shown in Figure 12e. The illustration of the electron-hole pairs is depicted in Figure 12f. Through this illustration, they demonstrated that the carriers generated by absorption layer could be transferred to the channel through the ligand.

The technology of multiphotocative QDs has also attracted attention recently in the field of phototransistors for sensing the visible light region and decreasing the PPC phenomenon.^[136,137] Han et al. showed a multi-photoactivated QDs/ZnO phototransistor.^[138] Figure 12g shows the fabrication process of the QD layer-by-layer patterning process to form multi-photoactive QDs under a patterned ZnO layer. Accordingly, the transfer curves of Figure 12h were obtained by irradiating 638, 520, and 405 nm light to the ZnO phototransistor. As a result, the generation of a photocurrent was verified by the rise of the off-current in the transfer curve and the negative shift of V_{th}. Figure 12i shows the endurance results of the phototransistor responding to a 1 Hz on and off signal of light at 638, 520, and 405 nm. Clearly, the amount of photocurrent was differed with exposure to different colors of light, and this difference was enough to distinguish the color of the visible light. Moreover, the PPC phenomenon of the metal oxide phototransistor almost disappeared.

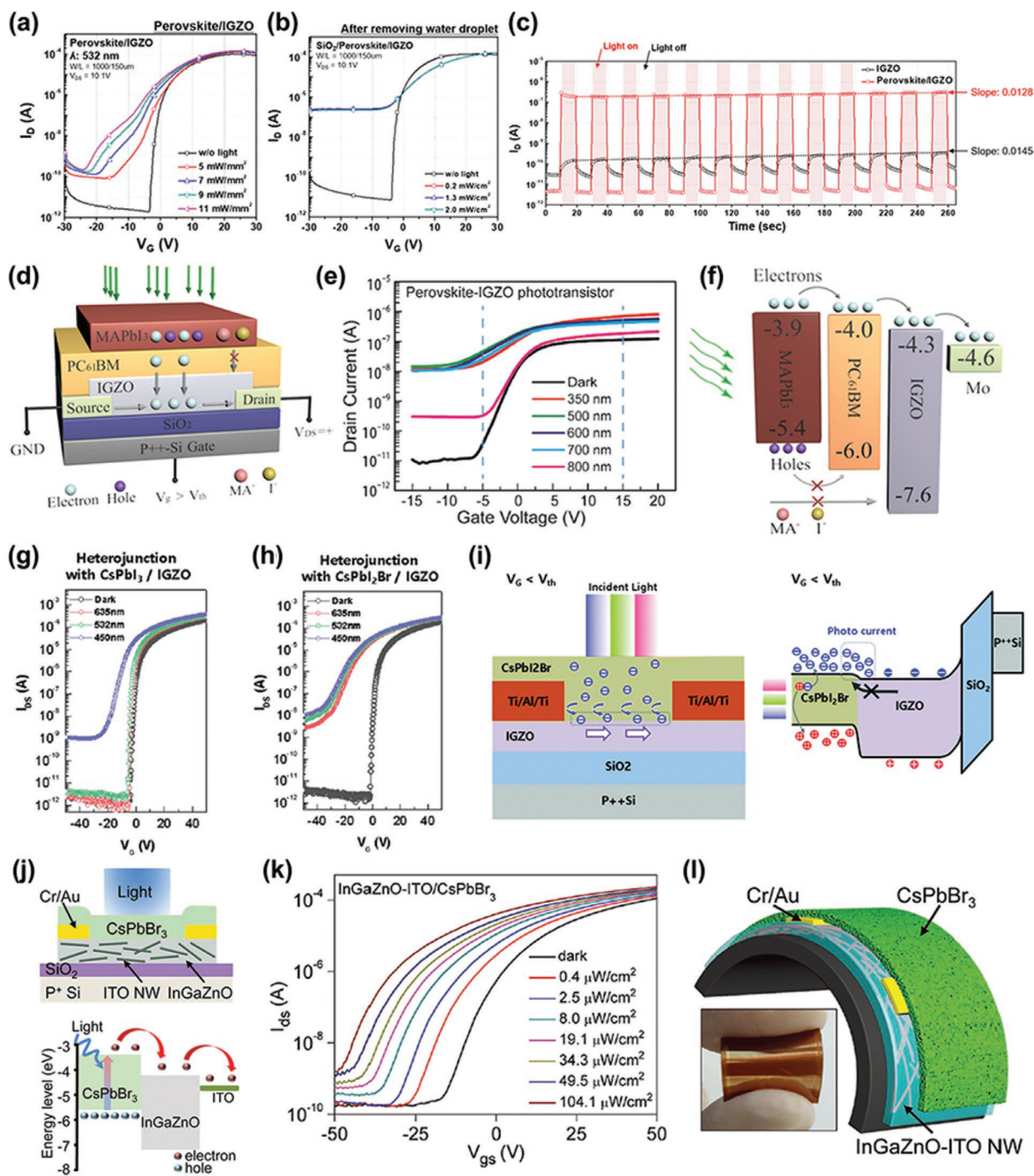


Figure 11. a) Transfer characteristics of perovskite/IGZO heterogeneous phototransistors under green laser (532 nm) illumination. b) Transfer characteristics of perovskite/IGZO heterogeneous phototransistor under light illumination after removing the water droplet. c) Transient response of perovskite/IGZO heterogeneous phototransistors over time under green laser (532 nm) illumination. a–c) Reproduced with permission.^[120] Copyright 2018, American Chemical Society. d) Schematic illustration of photo detection mechanism of perovskite/IGZO hybrid phototransistors under negative gate bias. e) Transfer characteristics of perovskite/IGZO hybrid phototransistors under light illumination with various wavelength. f) Schematic illustration of the energy band diagram of MAPbI₃, PC₆₁BM, IGZO, and charge transportation. d–f) Reproduced with permission.^[123] Copyright 2018, American Chemical Society. g) Transfer characteristics of heterojunction phototransistor with CsPbI₃/IGZO, and h) with CsPbI₂Br/IGZO at various wavelength of light irradiation. i) Schematic illustration of energy band diagram in CsPbI₂Br/IGZO heterojunction phototransistor at $V_G < V_{th}$ under light illumination. g–i) Reproduced with permission.^[124] Copyright 2019, Royal Society of Chemistry. j) Schematic diagrams of perovskite/IGZO-ITO heterojunction phototransistor and band diagram of the perovskite/IGZO-ITO heterostructure and photocarrier transfer under light illumination. k) Transfer characteristics of perovskite/IGZO-ITO phototransistors under 457 nm laser illumination. l) Schematic illustration of the flexible perovskite/IGZO-ITO phototransistor structure. Inset shows the optical image of devices fabricated on polyimide substrate. j–l) Reproduced with permission.^[125] Copyright 2020, Wiley-VCH.

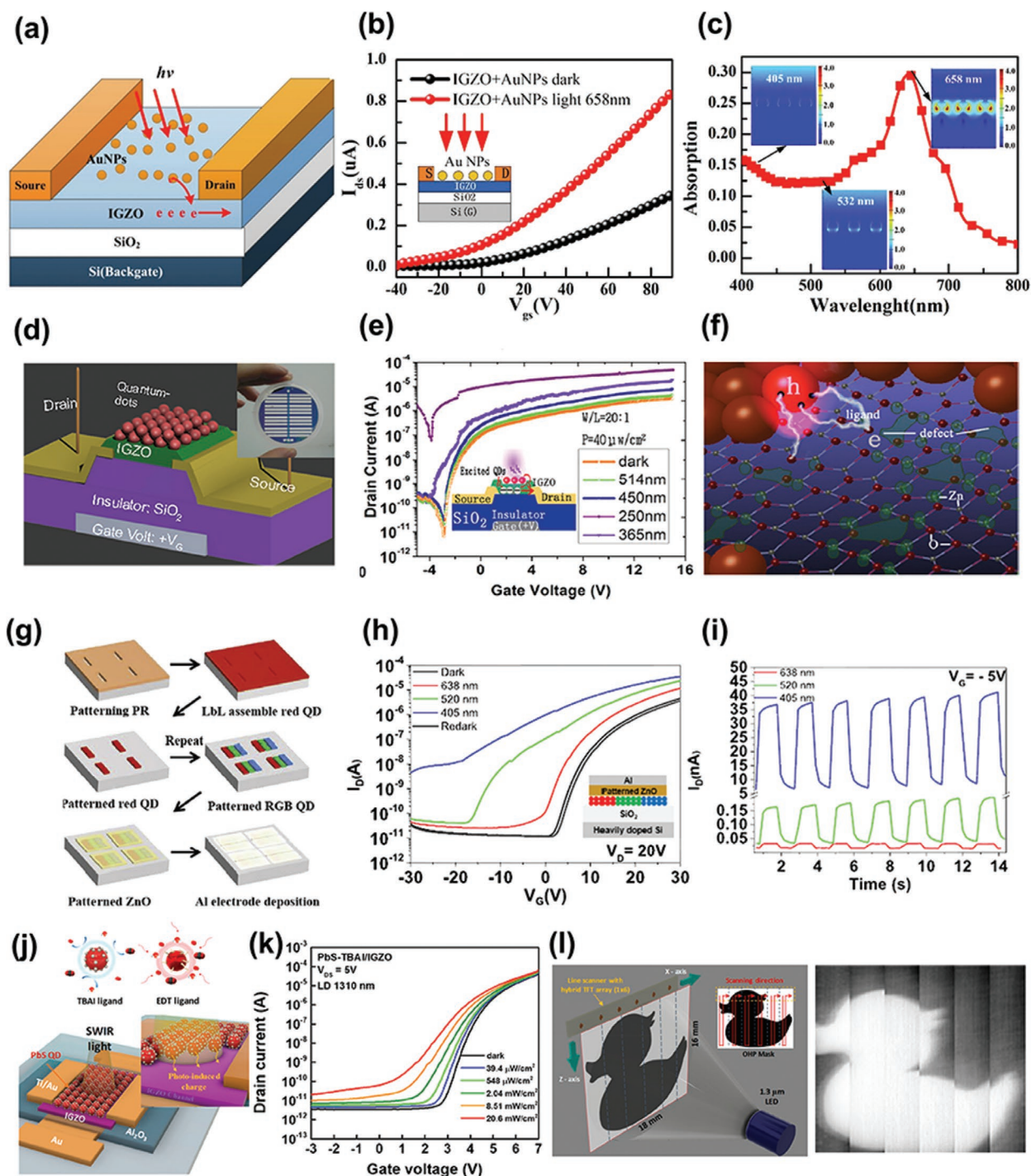


Figure 12. a) Schematic illustration of Au NPs/IGZO phototransistor. b) Transfer curves of the bare IGZO phototransistor under dark and light illumination. c) The simulated absorption curve of the Au NPs/IGZO film and the inset shows the electric field distribution at different wavelength. a–c) Reproduced with permission.^[128] Copyright 2019, Elsevier Inc. d) Schematic illustration of the device structure and the photography of the photoinduced TFT (inset). e) Transfer character of QDs/IGZO phototransistor under dark and light illumination. f) Schematic diagram of the atom structure, the electron-hole pairs excited by incident photons. d–f) Reproduced with permission.^[135] Copyright 2014, American Institute of Physics. g) Schematic of the QD layer-by-layer patterning process to form multi-photoactive channels under patterned ZnO. h) Transfer characteristics of the ZnO phototransistor with multi-photoactive QD layer under exposure of light of various wavelengths. The inset shows a schematic of the phototransistor under exposure of a 1 Hz periodic light signal. The light intensity is 100 μ W and the gate voltage is -5 V. i) Endurance test of the phototransistor under exposure of a 1 Hz periodic light signal. The light intensity is 100 μ W and the gate voltage is -5 V. g–i) Reproduced with permission.^[138] Copyright 2019, Elsevier Inc. j) Schematic illustration of PbS-TBAI/ZnO phototransistor. k) Photoinduced (and dark) transfer characteristics of the PbS-TBAI/IGZO phototransistor under 1310 nm illumination with different optical power density. l) Schematic diagram of the imaging process and the output image gain with a 1310 nm SWIR PbS-TBAI/IGZO flat-panel imager (1×6 line scanner). j–l) Reproduced with permission.^[139] Copyright 2020, American Chemical Society.

Table 2. Reports on the photosensing characteristics according to the materials of absorption layer using the metal oxide phototransistor.

Category	Figure	Absorption layer	Channel layer	Detection wavelength [nm]	PR [A W ⁻¹]	<i>P</i>	<i>D</i> * [Jones]	EQE [%]	Ref.	Published year
Chalcogenide	9a–c	MoS ₂	IGZO	405–980	1.7	–	–	–	[98]	2016
	9d,e	CdS	IGZO	550	–	–	5 × 10 ¹²	–	[100]	2017
	9f,g	Se	IGZO	405–635	1.39 × 10 ³	4.39 × 10 ⁹	3.44 × 10 ¹³	3.52 × 10 ³	[103]	2020
	–	CdS	IZO	445–650	0.0542	–	–	–	[102]	2014
	–	MoS ₂	IGZO	300–1500	0.0149	≈10 ⁵	2.73 × 10 ¹¹	–	[99]	2017
	–	CdS	ZTO	450–650	128	8.5 × 10 ⁶	4.1 × 10 ¹²	–	[101]	2018
Organic	10a–c	P3HT	IGZO	400–700	4	–	–	–	[109]	2010
	10d–f	PEDOT:PSS	SnO/IGZO	320–550	984	–	3.3 × 10 ¹⁴	≈10 ⁷	[110]	2015
	10g–j	PBDTT-DPP	IGZO	400–780	–	–	3.9 × 10 ¹²	1.62 × 10 ²	[113]	2015
	–	PBDTT-DPP:PC ₇₁ BM	ZnO/ZnON	380–940	1.7 × 10 ²	–	>10 ¹²	3.3 × 10 ¹⁴	[112]	2016
	–	D102 (dye)	In ₂ O ₃	400–700	2 × 10 ³	1 × 10 ⁶	–	–	[106]	2016
	–	C ₂₉ H ₃₀ F ₆ N ₄ O ₅ (empirical formula)	IZO	500–1400	≈10 ²	–	5 × 10 ¹²	≈10 ³	[107]	2019
	–	C ₇₀ /DBP	IGZO	625	0.05	>10 ⁴	–	–	[111]	2020
Perovskite	11a–c	MAPbI ₃	IGZO	400–750	61	3.3 × 10 ⁶	9.42 × 10 ¹⁰	154	[120]	2018
	11d–f	MAPbI ₃	IGZO	450–700	0.244	–	1.35 × 10 ¹²	–	[123]	2018
	11g–i	CsPbI ₂ Br ₂	IGZO	450–635	26.48	8.71 × 10 ⁶	8.42 × 10 ¹⁴	51	[124]	2019
	11j–l	CsPbBr ₃	ITO/IGZO	457	4.9 × 10 ⁶	–	7.6 × 10 ¹³	57	[125]	2020
	–	MAPbI ₃	IGZO	385–850	0.025	–	9.5 × 10 ⁹	–	[121]	2017
	–	MAPbI ₃	SnO	365–655	1.83 × 10 ³	–	2.11 × 10 ¹³	–	[122]	2019
Nanodot	12a–c	Au	IGZO	405–658	–	–	–	–	[128]	2019
	12d–f	CdSe	IGZO	450–514	≈10 ⁴	–	–	≈10 ⁴	[135]	2014
	12g–i	CdSe	ZnO	405–638	137	–	–	–	[138]	2019
	12j–l	PbS	IGZO	700–1310	10 ³ ≈ 10 ⁴	–	–	~10 ¹²	[139]	2020
	–	Ag	IGZO	405–780	≈5.5 × 10 ³	–	–	~1.2 × 10 ⁴	[126]	2015
	–	Graphene dot	IGZO	340–500	897	10 ⁶	–	–	[133]	2015
	–	CdSe	IGZO	405–635	1.35 × 10 ⁴	–	–	2.59 × 10 ⁴	[130]	2015
	–	Graphene QD	IGZO	270–400	–	–	–	–	[132]	2016
	–	PL-QD-O-640/560/440	ZnO	405–780	2.6 × 10 ⁻⁴	–	–	9.1 × 10 ⁻⁴	[137]	2018
	–	PbS, CdSe, CdS	IGZO	365–1310	>8.3 × 10 ³	–	4.2 × 10 ¹⁷	>60	[136]	2019
–	CdSe	IGZO	532	1.1 × 10 ⁴	–	5.3 × 10 ¹⁷	44	[129]	2020	
–	CdSe/ZnS	ZnO	405–780	–	–	–	–	[131]	2020	

Finally, we briefly introduce the main application of QDs/oxide-phototransistors-based short-wave infrared (SWIR) imagers. Hwang et al. reported a PbS-QD/IGZO-based hybrid phototransistor and a flat-panel SWIR imager.^[139] Figure 12j shows a schematic illustration view of the QD/IGZO phototransistor. In this study, two ligands, tetrabutylammonium iodide (TBAI) and ethanedithiol (EDT), which have been widely employed for PbS-QD-based devices, were selected. Figure 12k

shows dark and photoinduced transfer curves under 1310 nm SWIR illumination with different optical power densities. Through these curves, the QD-based phototransistors could detect SWIR region. Furthermore, this study demonstrated a prototype 1300 nm SWIR flat-panel image sensor array (as shown in Figure 12l).

Table 2 summarizes the properties of the metal oxide phototransistors according to the type of material of absorption layer.

Sensing wavelengths and optoelectronic parameters were classified and compared according to the chalcogenide, organic, perovskite, and nanodot materials used as the absorber material.

4. Future Convergence Technology Based on Metal Oxide Phototransistors

Recently, researchers have attempted to expand oxide phototransistors to a convergence technology incorporating bio, display, memory, and neuromorphic fields, rather than simply researching unit devices. Representative studies in each field are as follows:

4.1. Healthcare System

Researchers have recently attempted to use phototransistors in the field of biotechnology.^[140] Park et al. presented phototransistor arrays with QD/IGZO hybrid structures using QD materials of PbS, CdSe, and CdS, and attempted to apply the sensor arrays to biotechnology.^[136] The arrays capable of absorbing IR, red, green, and blue light were fabricated using different QD materials for each wavelength. This allows flexible sensor arrays to be wrapped around the finger and measured pulses by detecting changes in the LED light transmitted through the finger, as shown in **Figure 13a**.

4.2. Image Sensor on Panel

A convergence study was also conducted in which phototransistors were applied to display panels.^[79] Nathan et al. conducted a study to embed phototransistors inside the pixel of display panels, as shown in **Figure 13b**.^[91] IZO/GIZO-based metal oxide phototransistors were embedded in the pixel of in-cell touch panel to implement interactive displays. In particular, the metal oxide phototransistor, which has a higher photocurrent than the a-Si-based phototransistor, could eliminate the storage capacitor and the select switch TFT, and a simplified circuit could be constructed.

4.3. Photo Memory

Artificial visual perception systems have been attracted attention because they can enable the perception process such as recognition, learning, and memorization in the next generation robotics and human-like sensory electronics.^[141–145] Especially, some studies have focused on metal-oxide-based visual perception systems. For example, Shen et al. reported visual memory array with the In_2O_3 and Al_2O_3 layers, which was designed to mimic human visual memory by integrating UV image sensor arrays and resistance-switching memristors in series as shown in **Figure 13c**.^[146] Through this system, they successfully demonstrated that a butterfly shaped pattern could be observed from the mapping that read from the visual memory arrays, demonstrating the feasibility of imaging and memorizing when subjected to external stimulation of patterned light.

4.4. Photoinduced Neuromorphic

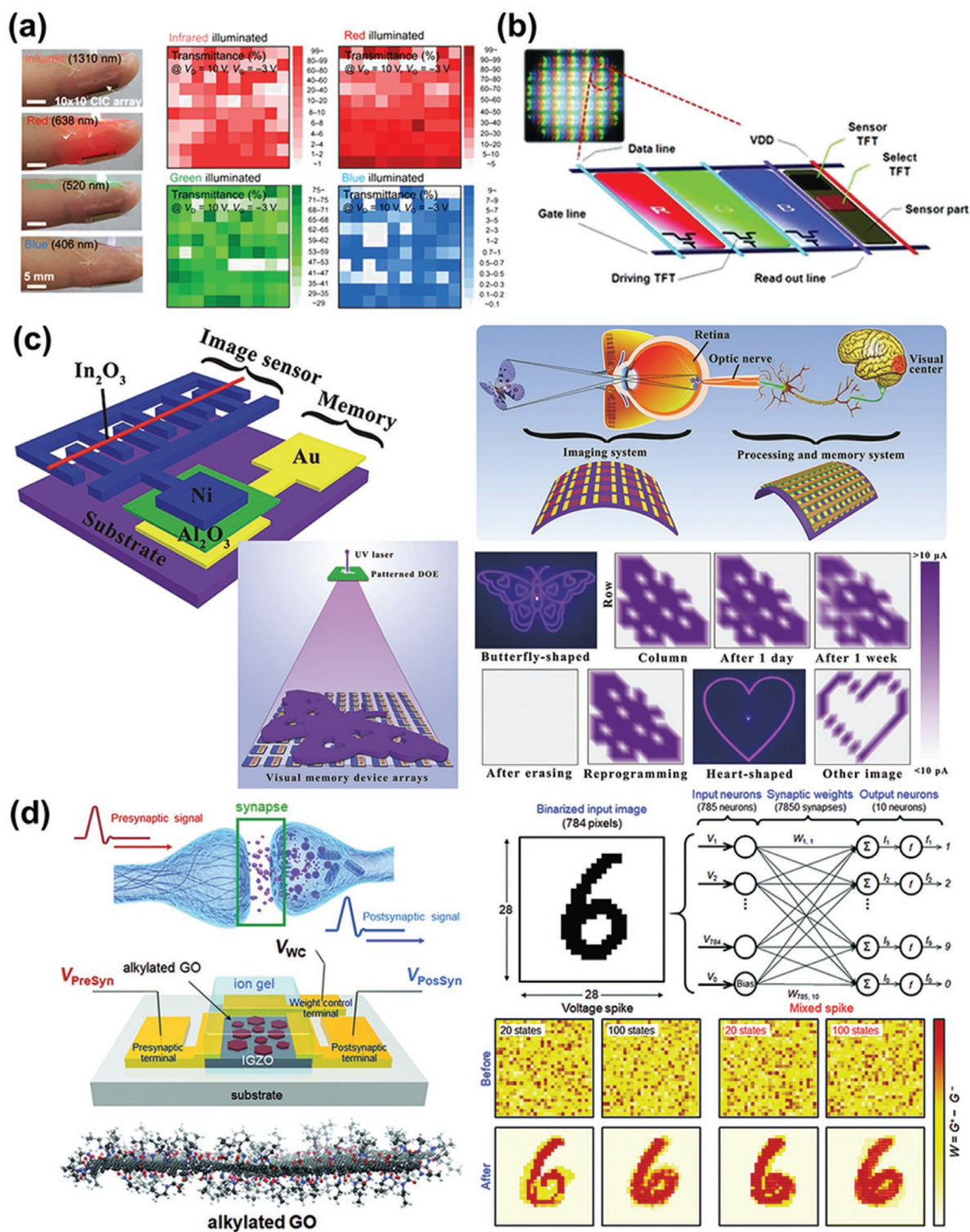
Recently, a photoinduced neuromorphic device was developed based on metal oxide semiconductors.^[147–152] Park et al. constructed the synaptic device using graphene oxide nanosheets modified with long alkyl chains embedded as a charge-trapping layer on the IGZO TFTs as shown in **Figure 13d**.^[153] As a result, the device exhibited the neuromorphic characteristics according to the light absorption of the device, and its reaction was visualized. The proposed photoinduced neuromorphic device is expected to play a key role in the implementation of neuromorphic computing based on optoelectronics.

In addition to the previously reported studies as above, the unique characteristics of oxide semiconductors will allow the phototransistors to be fused into more technical fields. The large area, low power consumption, and transparency, which are the distinctive features of oxide semiconductors, are expected to give functions that were difficult to implement with existing silicon- and organic-materials-based photosensors. It would be desirable if researchers are interested in these characteristics and refer to developing new applications in the future.

5. Conclusion and Outlook

In summary, as research on metal oxide TFTs has developed, their applications in phototransistors are being actively conducted. Broadening the light-sensing wavelength range and improving the PPC phenomenon have been major research topics over the past ten years. Researchers have made considerable progress in overcoming the limitations of metal oxide phototransistors by introducing absorption layer based on various materials such as oxide, chalcogenide, organic, perovskite, and nanodot, as shown in **Figure 14**. In 2012, Weng et al. developed a phototransistor based on a single IGZO channel with a detection wavelength of 250–400 nm and photoresponsivity of 4.75 A W^{-1} .^[70] And as a result of the considerable progress of research over time, in 2019, Park et al. developed IGZO phototransistors based on nanodot absorption layers with a detection range of 365–1310 nm and a photoresponsivity of $8.3 \times 10^3 \text{ A W}^{-1}$.^[136] In addition, researchers have attempted to use oxide phototransistors in new technology areas such as the field of biotechnology and in the development of displays, photo memory, and neuromorphic devices.

In the future, we propose that researchers develop various novel oxide thin-film treatment methods or alternative absorption layer materials that can improve the detection wavelength over a wide range and can reduce the PPC phenomenon. In particular, although studies have greatly improved light detection in the visible light region, there are still limited studies on IR detection with metal oxide phototransistors. In addition, research is needed to reduce the PPC phenomenon without supplying external activation energy. Although it is known that the PPC can be sufficiently improved with the gate pulse signal from the results of the research so far, if the PPC can be improved without supplying additional energy, improved utilization such as low power consumption devices or circuit simplification within the device will be possible. By solving the problems presented, we believe that metal oxide



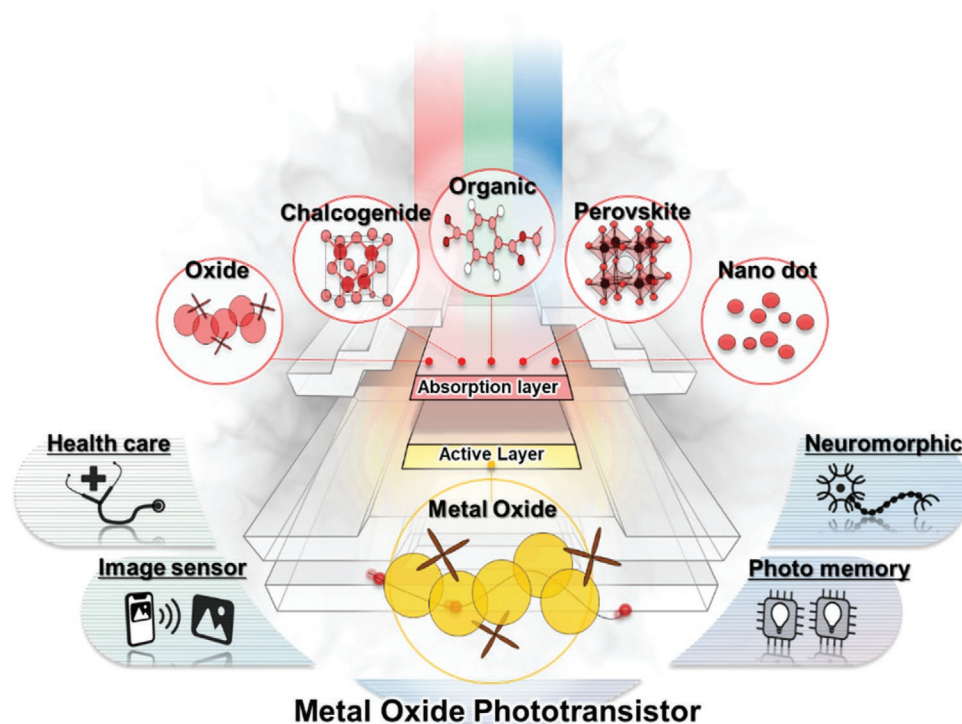


Figure 14. Summary of methods for overcoming the limitations of metal oxide phototransistors and their application to new technology fields.

phototransistors will become core sensor technology for the next generation of IoT for the 4th industrial revolution in the near future.

Supporting Information

Supporting Information is available from the Wiley Online Library or from the author.

Acknowledgements

H.Y. and I.S.L. contributed equally to this work. This research was supported by the National Research Foundation of Korea (NRF) Grant funded by the Korea Government (MSIT) (no. 2020M3H4A1A02084895).

Conflict of Interest

The authors declare no conflict of interest.

Keywords

light-absorption materials, oxide semiconductors, photosensors, phototransistors

Received: September 6, 2020
Revised: October 15, 2020
Published online: May 28, 2021

- [1] J. Bardeen, W. H. Brattain, *Phys. Rev.* **1948**, 74, 230.
- [2] A. Nathan, A. Kumar, K. Sakariya, P. Servati, S. Sambandan, D. Striakhilev, *IEEE J. Solid-State Circuits* **2004**, 39, 1477.
- [3] W. S. Wong, S. E. Ready, P. J. Lu, R. A. Street, *IEEE Electron Device Lett.* **2003**, 24, 577.
- [4] X. Gao, L. Lin, Y. Liu, X. Huang, *J. Disp. Technol.* **2015**, 11, 666.
- [5] K. Jang, Y. Kim, P. D. Phong, Y. Lee, J. Park, J. Yi, *Materials* **2019**, 12, 161.
- [6] M. L. Chabinyk, A. Salleo, *Chem. Mater.* **2004**, 16, 4509.
- [7] A. Liu, H. Zhu, W. T. Park, S. J. Kang, Y. Xu, M. G. Kim, Y. Y. Noh, *Adv. Mater.* **2018**, 30, 1802379.
- [8] H. Gleskova, S. Wagner, V. Gašparik, P. Kováč, *J. Electrochem. Soc.* **2001**, 148, G370.
- [9] S. Martin, C. S. Chiang, J. Y. Nahm, T. Li, J. Kanicki, Y. Ugai, *Jpn. J. Appl. Phys.* **2001**, 40, 530.
- [10] K. Nomura, H. Ohta, A. Takagi, T. Kamiya, M. Hirano, H. Hosono, *Nature* **2004**, 432, 488.
- [11] J. Sheng, E. J. Park, B. Shong, J. S. Park, *ACS Appl. Mater. Interfaces* **2017**, 9, 23934.
- [12] H. Yoo, Y. J. Tak, W. G. Kim, Y. G. Kim, H. J. Kim, *J. Mater. Chem. C* **2018**, 6, 6187.
- [13] D. B. Ruan, P. T. Liu, M. C. Yu, T. C. Chien, Y. C. Chiu, K. J. Gan, S. M. Sze, *ACS Appl. Mater. Interfaces* **2019**, 11, 22521.
- [14] W. K. Min, S. P. Park, H. J. Kim, J. H. Lee, K. Park, D. Kim, K. W. Kim, H. J. Kim, *ACS Appl. Mater. Interfaces* **2020**, 12, 24929.
- [15] I. S. Lee, Y. J. Tak, B. H. Kang, H. Yoo, S. Jung, H. J. Kim, *ACS Appl. Mater. Interfaces* **2020**, 12, 19123.
- [16] H. S. Jeong, M. J. Park, S. H. Kwon, H. J. Joo, H. I. Kwon, *Sens. Actuators, B* **2019**, 288, 625.
- [17] S. J. Kim, J. Jung, K. W. Lee, D. H. Yoon, T. S. Jung, S. R. Dugasani, S. H. Park, H. J. Kim, *ACS Appl. Mater. Interfaces* **2013**, 5, 10715.
- [18] S. J. Ding, X. Wu, *Chem. Mater.* **2020**, 32, 1343.

- [19] S. Vishniakou, R. Chen, Y. G. Ro, C. J. Brennan, C. Levy, E. T. Yu, S. A. Dayeh, *Adv. Mater. Technol.* **2018**, *3*, 1700279.
- [20] S. M. Lee, S. J. Park, K. H. Lee, J. S. Park, S. Park, Y. Yi, S. J. Kang, *Appl. Phys. Lett.* **2015**, *106*, 031112.
- [21] L. Shao, H. Wang, Y. Yang, Y. He, Y. Tang, H. Fang, J. Zhao, H. Xiao, K. Liang, M. Wei, W. Xu, M. Luo, Q. Wan, W. Hu, T. Gao, Z. Cui, *ACS Appl. Mater. Interfaces* **2019**, *11*, 12161.
- [22] N. Perea-López, A. L. Elías, A. Berkdemir, A. Castro-Beltran, H. R. Gutiérrez, S. Feng, R. Lv, T. Hayashi, F. López-Urías, S. Ghosh, B. Muchharla, S. Talapatra, H. Terrones, M. Terrones, *Adv. Funct. Mater.* **2013**, *23*, 5510.
- [23] D. Zhang, L. Gan, Y. Cao, Q. Wang, L. Qi, X. Guo, *Adv. Mater.* **2012**, *24*, 2715.
- [24] B. H. Kang, S. J. Jung, S. Hong, I. S. Lee, S. Hong, S. Kim, H. J. Kim, *J. Inf. Disp.* **2020**, *21*, 123.
- [25] L. Sang, M. Liao, M. Sumiya, *Sensors* **2013**, *13*, 10482.
- [26] M. Ahmadi, T. Wu, B. Hu, *Adv. Mater.* **2017**, *29*, 1605242.
- [27] N. Li, Z. Lan, L. Cai, F. Zhu, *J. Mater. Chem. C* **2019**, *7*, 3711.
- [28] P. C. Y. Chow, T. Someya, *Adv. Mater.* **2020**, *32*, 1902045.
- [29] A. V. Barve, S. J. Lee, S. K. Noh, S. Krishna, *Laser Photonics Rev.* **2010**, *4*, 738.
- [30] J. W. Park, B. H. Kang, H. J. Kim, *Adv. Funct. Mater.* **2020**, *30*, 1904632.
- [31] Y. S. Rim, H. Chen, B. Zhu, S. -H. Bae, S. Zhu, P. J. Li, I. C. Wang, Y. Yang, *Adv. Electrode Mater.* **2017**, *4*, 1700020.
- [32] T. Kamiya, H. Hosono, *NPG Asia Mater* **2010**, *2*, 15.
- [33] H. Oh, S. M. Yoon, M. K. Ryu, C. S. Hwang, S. Yang, S. H. K. Park, *Appl. Phys. Lett.* **2010**, *97*, 183502.
- [34] Y. Wang, C. Chen, T. Zou, L. Yan, C. Liu, X. Du, S. Zhang, H. Zhou, *Adv. Mater. Technol.* **2020**, *5*, 1900752.
- [35] D.-G. Kim, J.-U. Kim, J.-S. Lee, K.-S. Park, Y.-G. Chang, M.-H. Kim, *RSC Adv.* **2019**, *9*, 20865.
- [36] J. Sheng, T. Hong, H.-M. Lee, K. Kim, M. Sasase, J. Kim, H. Hosono, J.-S. Park, *ACS Appl. Mater. Interfaces* **2019**, *11*, 40300.
- [37] M. Li, J. Zheng, H. Xu, Z. Wang, Q. Wu, B. Huang, H. Zhou, C. Liu, *Adv. Mater. Interfaces* **2018**, *5*, 1700981.
- [38] H. Yu, H.-J. Kwon, X. Tang, D. Y. Lee, S. Nam, S. H. Kim, *Nanomaterials* **2020**, *10*, 1304.
- [39] H. N. Shah, R. Jayaganthan, D. Kaur, R. Chandra, *Thin Solid Films* **2010**, *518*, 5762.
- [40] W. Gulbinski, *Surf. Coat. Technol.* **2000**, *127*, 203.
- [41] A. E. Danks, S. R. Hall, Z. Schnepf, *Mater. Horiz.* **2016**, *3*, 91.
- [42] Y. Choi, G. H. Kim, W. H. Jeong, H. J. Kim, B. D. Chin, J.-W. Yu, *Thin Solid Films* **2010**, *518*, 6249.
- [43] K. J. Baeg, M. Binda, D. Natali, M. Caironi, Y. Y. Noh, *Adv. Mater.* **2013**, *25*, 4267.
- [44] R. Saran, R. J. Curry, *Nat. Photonics* **2016**, *10*, 81.
- [45] T. Agostinelli, M. Caironi, D. Natali, M. Sampietro, P. Biagioni, M. Finazzi, L. Duo, *J. Appl. Phys.* **2007**, *101*, 114504.
- [46] Y. Wakayama, R. Hayakawa, H.-S. Seo, *Sci. Technol. Adv. Mater.* **2014**, *15*, 024202.
- [47] S. O. Kasap, *Principles of Electronic Materials and Devices*, McGraw-Hill Education, New York **2006**.
- [48] D. Xiang, C. Han, J. Zhang, W. Chen, *Sci. Rep.* **2014**, *4*, 4981.
- [49] S. E. Ahn, S. Jeon, Y. W. Jeon, C. Kim, M. J. Lee, C. W. Lee, J. Park, I. Song, A. Nathan, S. Lee, U. I. Chung, *Adv. Mater.* **2013**, *25*, 5549.
- [50] H. Lee, J. Kim, S. K. Kim, Y. Lee, J. Y. Kim, J. T. Jang, J. Park, S. J. Choi, D. H. Kim, D. M. Kim, *IEEE Electron Device Lett.* **2017**, *38*, 584.
- [51] M. G. Yun, Y. K. Kim, C. H. Ahn, S. W. Cho, W. J. Kang, H. K. Cho, Y. H. Kim, *Sci. Rep.* **2016**, *6*, 31991.
- [52] M. A. Romero, M. A. G. Martinez, P. R. Herczfeld, *IEEE Trans. Microwave Theory Tech.* **1996**, *44*, 2279.
- [53] A. J. Seeds, A. A. A. Desalles, *IEEE Trans. Microwave Theory Tech.* **1990**, *38*, 577.
- [54] S. M. Sze, K. K. Ng, *Physics of Semiconductor Devices*, Wiley-Interscience, New Jersey **2007**.
- [55] C. S. Choi, H. S. Kang, W. Y. Choi, H. J. Kim, W. J. Choi, D. H. Kim, K. C. Jang, K. S. Seo, *IEEE Photonics Technol. Lett.* **2003**, *15*, 846.
- [56] H. S. Kang, C. S. Choi, W. Y. Choi, D. H. Kim, K. S. Seo, *Appl. Phys. Lett.* **2004**, *84*, 3780.
- [57] Y. F. Xu, P. R. Berger, J. N. Wilson, U. H. F. Bunz, *Appl. Phys. Lett.* **2004**, *85*, 4219.
- [58] Y. Fang, A. Armin, P. Meredith, J. Huang, *Nat. Photonics* **2019**, *13*, 1.
- [59] Z. Wu, Y. Zhai, H. Kim, J. D. Azoulay, T. N. Ng, *Acc. Chem. Res.* **2018**, *51*, 3144.
- [60] R. H. Bube, *Photoconductivity of Solids*, John Wiley & Sons, Inc., New York **1960**.
- [61] X. Zhou, D. Yang, D. Ma, A. Vadim, T. Ahamad, S. M. Alshehri, *Adv. Funct. Mater.* **2016**, *26*, 6619.
- [62] G. Konstantatos, A. Fischer, E. Klem, J. Clifford, S. Hoogland, E. H. Sargent, L. Levina, I. Howard, *Nature* **2006**, *442*, 180.
- [63] Y. Zhang, D. J. Hellebusch, N. D. Bronstein, C. Ko, D. F. Ogletree, M. Salmeron, A. P. Alivisatos, *Nat. Commun.* **2016**, *7*, 11924.
- [64] L. Nian, W. Zhang, N. Zhu, L. Liu, Z. Xie, H. Wu, F. Würthner, Y. Ma, *J. Am. Chem. Soc.* **2015**, *137*, 6995.
- [65] G. Konstantatos, E. H. Sargent, *Appl. Phys. Lett.* **2007**, *91*, 173505.
- [66] K. Ghaffarzadeh, A. Nathan, J. Robertson, S. Kim, S. Jeon, C. Kim, U. I. Chung, J. H. Lee, *Appl. Phys. Lett.* **2010**, *97*, 143510.
- [67] J. Jang, Y. Kang, D. Cha, J. Bae, S. Lee, *Crystals* **2019**, *9*, 192.
- [68] S. Jeon, S. E. Ahn, I. Song, C. J. Kim, U. I. Chung, E. Lee, I. Yoo, A. Nathan, S. Lee, K. Ghaffarzadeh, J. Robertson, K. Kim, *Nat. Mater.* **2012**, *11*, 301.
- [69] B. H. Kang, W. G. Kim, J. Chung, J. H. Lee, H. J. Kim, *ACS Appl. Mater. Interfaces* **2018**, *10*, 7223.
- [70] T. H. Chang, C. J. Weng, W. Y. S. J. Chang, T. Y. Tsai, Z. D. Huang, *Appl. Phys. Lett.* **2012**, *101*, 261112.
- [71] M. Lee, M. Kim, J. W. Jo, S. K. Park, *Appl. Phys. Lett.* **2018**, *112*, 052103.
- [72] S. Park, N. K. Cho, B. J. Kim, S. Y. Jeong, I. K. Han, Y. S. Kim, S. J. Kang, *ACS Appl. Electron. Mater.* **2019**, *1*, 2655.
- [73] X. L. Wang, Y. Shao, X. Wu, M. N. Zhang, L. Li, W. J. Liu, S. J. Ding, *RSC Adv.* **2020**, *10*, 3572.
- [74] G. Han, S. Cao, Q. Yang, W. Yang, T. Guo, H. Chen, *ACS Appl. Mater. Interfaces* **2018**, *10*, 40631.
- [75] T. H. Chang, C. J. Chiu, S. J. Chang, T. Y. Tsai, Z. D. Huang, W. Y. Weng, *Appl. Phys. Lett.* **2013**, *102*, 221104.
- [76] H. Y. Liu, R. C. Huang, *IEEE Electron Device Lett.* **2018**, *40*, 243.
- [77] S. Knobelspies, A. Daus, G. Cantarella, L. Petti, N. Münzenrieder, G. Tröster, G. A. Salvatore, *Adv. Electrode. Mater.* **2016**, *2*, 1600273.
- [78] M. Ma, D. Zhang, Y. Li, R. Lin, W. Zheng, F. Huang, *ACS Appl. Electron. Mater.* **2019**, *1*, 1653.
- [79] P. T. Liu, D. B. Ruan, X. Y. Yeh, Y. C. Chiu, G. T. Zheng, S. M. Sze, *Sci. Rep.* **2018**, *8*, 8153.
- [80] J. Y. Li, S. P. Chang, M. H. Hsu, S. J. Chang, *Materials* **2017**, *10*, 126.
- [81] S. E. Ahn, S. Park, T. Kim, J. Park, S. Jeon, *J. Vac. Sci. Technol., B* **2015**, *33*, 031205.
- [82] J. H. Ahn, S. E. Ahn, Y. Jeon, S. Lee, I. Song, J. Kim, H. Choi, U. I. Chung, *Appl. Phys. Lett.* **2013**, *103*, 173515.
- [83] S. J. Chang, T. H. Chang, W. Y. Weng, C. J. Chiu, S. P. Chang, *IEEE J. Sel. Top. Quantum Electron.* **2014**, *20*, 125.
- [84] X. Liu, X. Liu, J. Wang, C. Liao, X. Xiao, S. Guo, C. Jiang, Z. Fan, T. Wang, X. Chen, W. Lu, W. Hu, L. Liao, *Adv. Mater.* **2014**, *26*, 7399.
- [85] J. D. Hwang, C. C. Yang, C. M. Chu, *ACS Appl. Mater. Interfaces* **2017**, *9*, 23904.
- [86] H. Choi, S. Seo, J. H. Lee, S. H. Hong, J. Song, S. Kim, S. Y. Yim, K. Lee, S. J. Park, S. Lee, *J. Mater. Chem. C* **2018**, *6*, 6014.
- [87] M. M. Y. A. Alsaif, S. Kuriakose, S. Walia, N. Syed, A. Jannat, B. Y. Zhang, F. Haque, M. Mohiuddin, T. Alkathiri, N. Pillai, T. Daeneke, J. Z. Ou, A. Zavabeti, *Adv. Mater. Interfaces* **2019**, *6*, 1900007.

- [88] I. S. Lee, D. Kim, S. Jung, B. H. Kang, H. J. Kim, *J. Inf. Disp.* **2020**, *21*, 217.
- [89] D. B. Ruan, P. T. Liu, Y. H. Chen, Y. C. Chiu, T. C. Chien, M. C. Yu, K. J. Gan, S. M. Sze, *Adv. Electron. Mater.* **2019**, *5*, 1800824.
- [90] S. Jeon, I. Song, S. Lee, B. Ryu, S. E. Ahn, E. Lee, B. Ryu, S. E. Ahn, E. Lee, Y. Kim, A. Nathan, J. Ronertson, U. I. Chung, *Adv. Mater.* **2014**, *26*, 7102.
- [91] S. E. Ahn, I. Song, S. Jeon, Y. W. Jeon, Y. Kim, C. Kim, B. Ryu, J. H. Lee, A. Nathan, S. Lee, G. T. Kim, U. I. Chung, *Adv. Mater.* **2012**, *24*, 2631.
- [92] J. Chung, Y. J. Tak, W. G. Kim, B. H. Kang, H. J. Kim, *ACS Appl. Mater. Interfaces* **2019**, *11*, 38964.
- [93] D. Kim, Y. G. Kim, B. H. Kang, J. H. Lee, J. Chung, H. J. Kim, *J. Mater. Chem. C* **2020**, *8*, 165.
- [94] J. Kim, T. H. Kim, S. Oh, J. H. Nam, H. Y. Jang, Y. Kim, N. Yamada, H. Kobayashi, S. Y. Kim, B. H. Lee, H. Habazaki, W. Park, B. Cho, *ACS Appl. Electron. Mater.* **2020**, *2*, 1478.
- [95] C. H. Ahn, W. J. Kang, Y. K. Kim, M. G. Yun, H. K. Cho, *ACS Appl. Mater. Interfaces* **2016**, *8*, 15518.
- [96] S. Qiao, J. Liu, X. Niu, B. Liang, G. Fu, Z. Li, S. Wang, K. Ren, C. Pan, *Adv. Funct. Mater.* **2018**, *28*, 1707311.
- [97] S. Kim, Y. C. Kim, Y. J. Choi, H. J. Woo, Y. J. Song, M. S. Kang, C. Lee, J. H. Cho, *ACS Appl. Mater. Interfaces* **2019**, *11*, 35444.
- [98] J. Yang, H. Kwak, Y. Lee, Y. S. Kang, M. H. Cho, J. H. Cho, Y. H. Kim, S. J. Jeong, S. Park, H. J. Lee, H. Kim, *ACS Appl. Mater. Interfaces* **2016**, *8*, 8576.
- [99] S. W. Park, D. Chu, D. Y. Song, S. K. Lee, E. K. Kim, *Nanotechnology* **2017**, *28*, 475206.
- [100] C. H. Ahn, Y. K. Kim, W. J. Kang, K. S. Kim, H. K. Cho, *J. Alloys Compd.* **2017**, *725*, 891.
- [101] S. W. Cho, Y. B. Kim, S. H. Jung, S. K. Baek, J. S. Kim, M. Lee, H. K. Cho, Y. H. Kim, *Adv. Opt. Mater.* **2018**, *6*, 1800196.
- [102] X. Liu, L. Jiang, X. Zou, X. Xiao, S. Guo, C. Jiang, X. Liu, Z. Fan, W. Hu, X. Chen, W. Lu, W. Hu, L. Liao, *Adv. Mater.* **2014**, *26*, 2919.
- [103] H. Yoo, W. G. Kim, B. H. Kang, H. T. Kim, J. W. Park, D. H. Choi, T. S. Kim, J. H. Lim, H. J. Kim, *ACS Appl. Mater. Interfaces* **2020**, *12*, 10673.
- [104] S. Mansouri, R. Bourguiga, A. A. Al-Ghamdi, F. Al-Hazmi, O. A. Al-Hartomy, F. El-Tantawy, F. Yakuphanoglu, *Synth. Met.* **2012**, *162*, 1681.
- [105] P. Pattanasattayavong, S. Rossbauer, S. Thomas, J. G. Labram, H. J. Snaith, T. D. Anthopoulos, *J. Appl. Phys.* **2012**, *112*, 074507.
- [106] A. D. Mottram, Y. H. Lin, P. Pattanasattayavong, K. Zhao, A. Amassian, T. D. Anthopoulos, *ACS Appl. Mater. Interfaces* **2016**, *8*, 4894.
- [107] H. Kim, Z. Wu, N. Eedugurala, J. D. Azoulay, T. N. Ng, *ACS Appl. Mater. Interfaces* **2019**, *11*, 36880.
- [108] T. M. Clarke, J. R. Durrant, *Chem. Rev.* **2010**, *110*, 6736.
- [109] H. W. Zan, W. T. Chen, H. W. Hsueh, S. C. Kao, M. C. Ku, C. C. Tsai, H. F. Meng, *Appl. Phys. Lett.* **2010**, *97*, 203506.
- [110] J. Yu, K. Javaid, L. Liang, W. Wu, Y. Liang, A. Song, H. Cao, *ACS Appl. Mater. Interfaces* **2018**, *10*, 8102.
- [111] Z. Chen, G. Sheleg, H. Shekhar, N. Tessler, *ACS Appl. Mater. Interfaces* **2020**, *12*, 15430.
- [112] Y. S. Rim, K. C. Ok, Y. M. Yang, H. Chen, S. H. Bae, C. Wang, Y. Yang, *ACS Appl. Mater. Interfaces* **2016**, *8*, 14665.
- [113] Y. S. Rim, Y. Yang, S. H. Bae, H. Chen, C. Li, M. S. Goorsky, Y. Yang, *Adv. Mater.* **2015**, *27*, 6885.
- [114] W. Peng, R. Yu, X. Wang, Z. Wang, H. Zou, Y. He, Z. L. Wang, *Nano Res.* **2016**, *9*, 3695.
- [115] X. Liu, Z. Tao, W. Kuang, Q. H. , Q. Li, J. Chen, W. Lei, *IEEE Electron Device Lett.* **2017**, *38*, 1270.
- [116] X. Hu, H. Zhou, Z. Jiang, X. Wang, S. Yuan, J. Lan, Y. Fu, X. Zhang, W. Zheng, X. Wang, X. Zhu, L. Liao, G. Xu, S. Jin, A. Pan, *ACS Nano* **2017**, *11*, 9869.
- [117] Z. Heydari, H. Abdy, M. Madani, M. P. Ghaziani, M. Kolehdoz, E. Asl-Soleimani, *J. Mater. Sci.: Mater. Electron.* **2020**, *31*, 154.
- [118] L. Yan, X. Du, C. Liu, S. Zhang, H. Zhou, *Phys. Status Solidi A* **2019**, *216*, 1900417.
- [119] Y. Wang, C. Chen, T. Zou, L. Yan, C. Liu, X. Du, S. Zhang, H. Zhou, *Adv. Mater. Technol.* **2020**, *5*, 1900752.
- [120] Y. J. Tak, D. J. Kim, W. G. Kim, J. H. Lee, S. J. Kim, J. H. Kim, H. J. Kim, *ACS Appl. Mater. Interfaces* **2018**, *10*, 12854.
- [121] S. Du, G. Li, X. Cao, Y. Wang, H. Lu, S. Zhang, C. Liu, H. Zhou, *Adv. Electron. Mater.* **2017**, *3*, 1600325.
- [122] X. Guan, Z. Wang, M. K. Hota, H. N. Alshareef, T. Wu, *Adv. Electron. Mater.* **2019**, *5*, 1800538.
- [123] X. Xu, L. Yan, T. Zhou, R. Qiu, C. Liu, Q. Dai, J. Chen, S. Zhong, H. Zhou, *ACS Appl. Mater. Interfaces* **2018**, *10*, 44144.
- [124] H. J. Na, N. K. Cho, J. Park, S. E. Lee, E. G. Lee, C. Im, Y. S. Kim, *J. Mater. Chem. C* **2019**, *7*, 14223.
- [125] Y. Hou, L. Wang, X. Zou, D. Wan, C. Liu, G. Li, X. Liu, Y. Liu, C. Jiang, J. C. Ho, L. Liao, *Small* **2020**, *16*, 1905609.
- [126] J. Yu, S. W. Shin, K. H. Lee, J. S. Park, *J. Vac. Sci. Technol., B* **2015**, *33*, 061211.
- [127] J. Yu, J. Cho, H. M. Lee, J. S. Park, *Jpn. J. Appl. Phys.* **2016**, *55*, 111101.
- [128] Y. Zhai, G. Chen, J. Ji, Z. Wu, Y. Li, Q. Wang, *Phys. E* **2019**, *113*, 92.
- [129] J. Kim, S. M. Kwon, C. Jo, J. S. Heo, W. B. Kim, H. S. Jung, S. K. Park, *ACS Appl. Mater. Interfaces* **2020**, *12*, 16620.
- [130] S. W. Shin, K. H. Lee, J. S. Park, S. J. Kang, *ACS Appl. Mater. Interfaces* **2015**, *7*, 19666.
- [131] B. J. Kim, N. K. Cho, S. Park, S. Jeong, D. Jeon, Y. Kang, S. J. Kang, *RSC Adv.* **2020**, *10*, 16404.
- [132] H. Zhu, A. Liu, F. Shan, W. Yang, W. Zhang, D. Li, J. Liu, *Carbon* **2016**, *100*, 201.
- [133] Z. Pei, H. C. Lai, J. Y. Wang, W. H. Chiang, C. H. Chen, *IEEE Electron Device Lett.* **2014**, *36*, 46.
- [134] H. Yu, X. Liu, L. Yan, T. Zou, H. Yang, C. Liu, H. Zhou, *Semicond. Sci. Technol.* **2019**, *34*, 125013.
- [135] X. Liu, X. Yang, M. Liu, Z. Tao, Q. Dai, L. Wei, A. Nathan, *Appl. Phys. Lett.* **2014**, *104*, 113501.
- [136] J. Kim, S. M. Kwon, Y. K. Kang, Y. H. Kim, M. J. Lee, K. Han, S. K. Park, *Sci. Adv.* **2019**, *5*, eaax8801.
- [137] J. Yu, B. J. Kim, S. Park, I. K. Han, S. J. Kang, *Jpn. J. Appl. Phys.* **2018**, *57*, 044001.
- [138] S. Cha, S. Jeong, B. J. Kim, S. J. Kang, Y. D. Kim, I. K. Han, *Curr. Appl. Phys.* **2019**, *19*, 992.
- [139] H. T. Choi, J.-H. Kang, J. Ahn, J. Jin, J. Kim, S. Park, Y.-H. Kim, H. Kim, J. D. Song, G. W. Hwang, S. Im, W. Shim, Y. T. Lee, M.-C. Park, D. K. Hwang, *ACS Photonics* **2020**, *7*, 1932.
- [140] D. Choi, M. Park, J. Jeong, H. B. Shin, Y. C. Choi, K. S. Jeong, *ACS Appl. Mater. Interfaces* **2019**, *11*, 7242.
- [141] D. G. Seo, Y. Lee, G. T. Go, M. Pei, S. Jung, Y. H. Jeong, W. Lee, H.-L. Park, S.-W. Kim, H. Yang, C. Yang, T.-W. Lee, *Nano Energy* **2019**, *65*, 104035.
- [142] R. Hinchet, H.-J. Yoon, H. Ryu, M.-K. Kim, E.-K. Chio, D.-S. Kim, S.-W. Kim, *Science* **2019**, *365*, 491.
- [143] Y.-B. Guo, L.-Q. Zhu, *Chin. Phys. B* **2020**, *29*, 078502.
- [144] G. J. Lee, C. Choi, D. H. Kim, Y. M. Song, *Adv. Funct. Mater.* **2018**, *28*, 1705202.
- [145] X. Yang, Z. Xiong, Y. Chen, Y. Ren, L. Zhou, H. Li, Y. Zhou, F. Pan, S.-T. Han, *Nano Energy* **2020**, *78*, 105246.
- [146] S. Chen, Z. Lou, D. Chen, G. Shen, *Adv. Mater.* **2018**, *30*, 1705400.
- [147] M. Lee, W. Lee, S. Choi, J.-W. Jo, J. Kim, S. K. Park, Y.-H. Kim, *Adv. Mater.* **2017**, *29*, 1700951.
- [148] M. R. Kulkarni, R. A. John, N. Tiwari, A. Nirmal, S. E. Ng, A. C. Nguyen, N. Marhevs, *Small* **2019**, *15*, 1901457.
- [149] M. R. Azghadi, Y.-C. Chen, J. K. Eshraghian, J. Chen, C.-Y. Lin, A. Amirsoleimani, A. Mehonic, A. J. Kenyon, B. Fowler, J. C. Lee, Y.-F. Chang, *Adv. Intell. Syst.* **2020**, *2*, 1900189.

[150] M. Prezioso, F. M. -Bayat, B. D. Hoskins, G. C. Adam, K. K. Likharev, D. B. Strukov, *Nature* **2015**, 521, 61.

[151] Y. Yang, Y. He, S. Nie, Y. Shi, Q. Wan, *IEEE Electron Device Lett.* **2018**, 39, 897.

[152] S. M. Kwon, S. W. Cho, M. Kim, J. S. Heo, Y. -H. Kim, S. K. Park, *Adv. Mater.* **2019**, 31, 1906433.

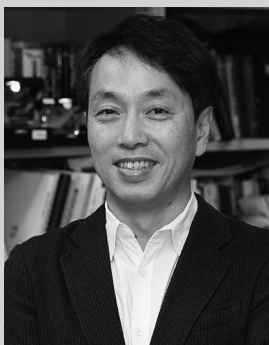
[153] J. Sun, S. Oh, Y. Choi, S. Seo, M. J. Oh, M. Lee, W. B. Lee, P. J. Yoo, J. H. Cho, J.-H. Park, *Adv. Funct. Mater.* **2018**, 28, 1804397.



Hyukjoon Yoo received his B.S. degree from the Institute of Physics and Applied Physics at Yonsei University, Seoul, South Korea, in 2017. He is currently a Ph.D. candidate in the School of Electrical and Electronic Engineering at the same institute. He has been conducting research on electrical characteristics and stability improvement of metal oxide TFTs, and metal-oxide-based sensors such as phototransistors.



I. Sak Lee received his B.S. degree from the Department of Electronic and Electrical Engineering at Dankook University, Gyeonggi-do, South Korea, in 2017. He is currently a Ph.D. candidate in the School of Electrical and Electronic Engineering at Yonsei University, Seoul, South Korea. He has been conducting research on high-performance n-type oxide TFTs and their application toward photosensors.



Hyun Jae Kim received his B.S. in 1991 from the School of Materials Science and Engineering, Yonsei University, and his M.S. and Ph.D. in 1993 and 1996 from the Department of Materials Science and Engineering, Columbia University. After being a principal engineer at Samsung Electronics from 1996 to 2005 and a visiting professor at Ecole Polytechnique from 2004 to 2005, he has been a professor of the School of Electrical and Electronic Engineering at Yonsei University since 2005. His research focuses on various electronic devices such as oxide TFTs, photosensors, biosensors, ReRAMs, and energy-storage devices.